A Numerical Study of the Mediterranean Sea Circulation

MARCO ZAVATARELLI* AND GEORGE L. MELLOR

Program in Atmospheric and Oceanic Sciences, Princeton University, Princeton, New Jersey

(Manuscript received 7 October 1992, in final form 12 August 1994)

ABSTRACT

A primitive equation ocean model that makes use of a curvilinear orthogonal grid and a sigma-coordinate system was used to simulate the Mediterranean Sea. The model was forced with monthly climatological values of wind stress, heat, and salinity flux. With the help of the curvilinear horizontal grid, the larger scales of the entire Mediterranean Sea are modeled, and the topography around the narrow and shallow Straits of Gibraltar is also reasonably well represented. The resulting model inflow and outflow seems to mimic the real Mediterranean, often in considerable detail. Levantine Intermediate Water is formed in the Levantine Basin and exits through the Strait of Sicily and the Strait of Gibraltar. Deep-water formation processes are clearly represented by the model.

The model results indicate that in the western Mediterranean the wind stress is very important in establishing the summer northward shift of the Atlantic inflow. Lateral boundary runoff, surface salinity, and heat fluxes are necessary for the maintenance of the cyclonic circulation in the northern Balearic Basin and enhance the seasonal reversal of the circulation in the Tyrrhenian Sea. An interesting result is the existence of a seasonal variation in the path of the Levantine Intermediate Water.

1. Introduction

This paper deals with model simulations of the general circulation of the Mediterranean Sea. An objective is to assess the degree to which the model mimics the real Mediterranean and various physical processes that have been observed. If confidence can be established in numerical models, then they can provide useful and detailed information not available from observations.

The Mediterranean Sea, as depicted in Fig. 1, is an enclosed basin connected to the Atlantic Ocean by the narrow Strait of Gibraltar, whose width is 13 km and sill depth is 300 m, and connected to the Black Sea by the Dardanelles/Marmara Sea/Bosphorus system. It is made up of two sub-basins, the Western (WMED) and the Eastern (EMED) Mediterranean, connected by the Strait of Sicily, whose width is about 35 km and whose sill depth is about 300 m.

With the exception of the Gulf of Lions, the continental shelves of the WMED are narrow. The Tyrrhenian Sea, between the Italian peninsula and the islands of Sardinia and Corsica, is the easternmost and deepest part of the basin, about 3500 m, and joins the rest of the WMED to the south in a wide opening between Sardinia and Sicily. The Balearic Sea, otherwise known as the Algero–Provencal Basin, at a depth of about 2500 m, occupies the central part of the basin and extends northeast to the Ligurian Sea and west towards the Alboran Sea and Gibraltar.

The EMED is more complicated than the WMED. Four sub-basins are seen in Fig. 1: the Ionian, the Levantine, the Adriatic, and the Aegean Seas. The Ionian Sea lies between Italy and Greece to the north, and Libya and Tunisia to the south and has a depth of about 3500–4000 m with a maximum of 5000 m south of Greece. The Levantine Sea has depths of about 2500–3000 m in the center of the basin and a maximum depth of about 4500 m in a depression located southeast of the island of Rhodes. It merges with the Ionian Sea through the Cretan Passage at a depth of about 1500 m between Crete and the Libyan coast. The Adriatic Sea is connected to the Ionian by the Strait of Otranto, whose width is about 75 km and sill depth is about 800 m; an extended continental shelf lies to the north and a relatively deep section is south of the strait. The northernmost end of the Adriatic and of the Mediterranean Sea is the Gulf of Venice. The Aegean Sea joins the Levantine Sea through several passages and straits, located between the Greek and Turkish coast and the islands of Crete and Rhodes, with sill depths ranging from 300 to 700 m and widths from 15 to 60 km. It has very irregular coastlines and topography with many islands. Its maximum depth is about 1500 m.

* Current affiliation: Istituto per lo Studio delle Metodologie Geofisico Ambientali, Modena, Italy.

Corresponding author address: Prof. George L. Mellor, Program in Atmospheric and Oceanic Sciences, Princeton University, Sayre Hall, P.O. Box CN710, Princeton, NJ 08544-0710.
E-mail: glm@splash.princeton.edu

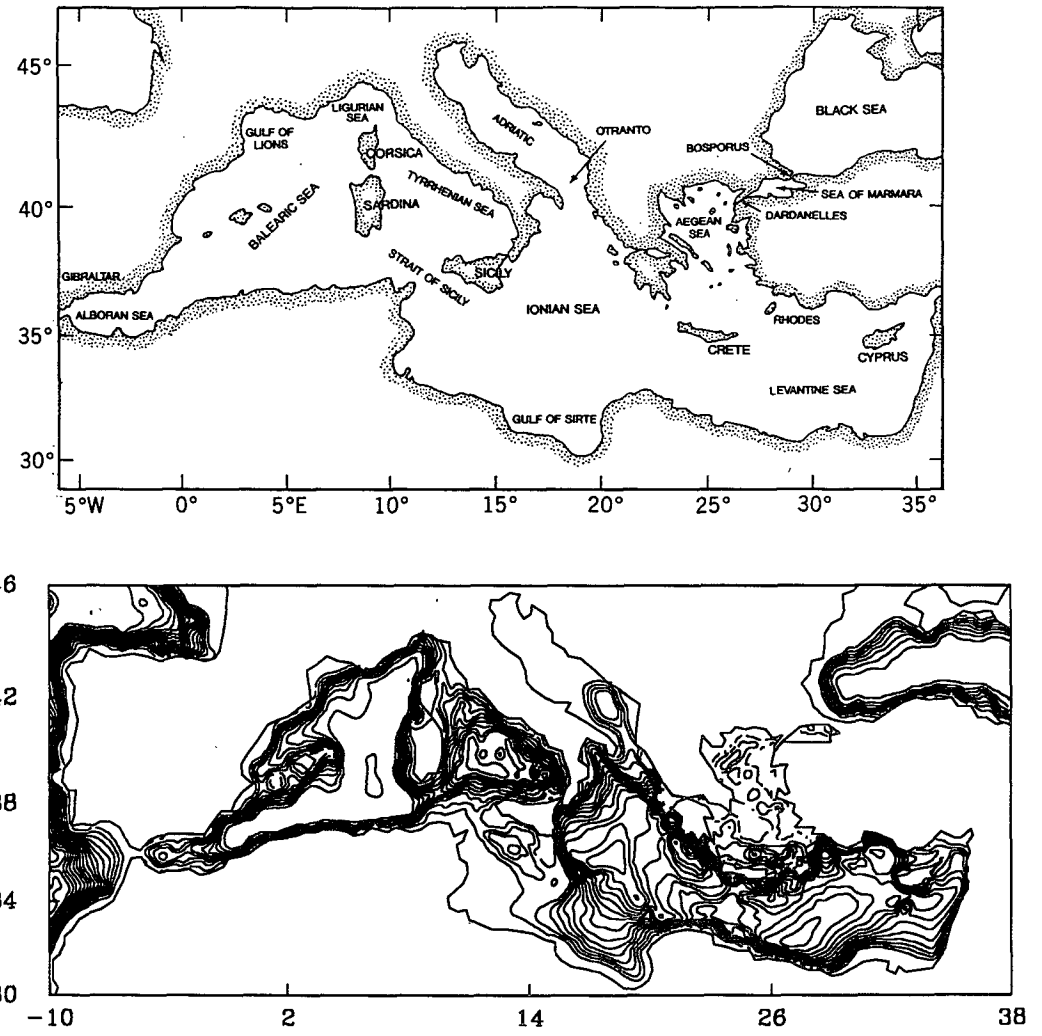

FIG. 1. The Mediterranean Sea. (Upper) Geographic features (adapted from Hopkins 1978); (lower) bathymetric map (U.S. Navy bathymetric database); the contour interval is 250 m.

There have been previous modeling studies of the Mediterranean. Studies with primitive equation models were carried out by Menzin and Moskalenko (1982), who restricted attention to the barotropic, wind-driven circulation. Stanev et al. (1989) used a coarse-resolution model to investigate the response of the circulation to annual and seasonal forcing whereas the work of Pinardi and Navarra (1993) focused on the wind-driven circulation in a basin with simplified bathymetry. Further calculations with increasingly complete and realistic forcing were carried out by Roussenov et al. (1994). An inverse model was used by Tziperman and Malanotte-Rizzoli (1991) to calculate the seasonal climatological circulation.

Regional circulation studies were carried out by Heburn (1987) with a one-layer, reduced gravity model of the western Mediterranean, by Beckers (1991) who applied the GHER model to the Western Mediterranean, by Malanotte-Rizzoli and Bergamasco (1989, 1991) and Bergamasco et al. (1993) who performed an extensive set of experiments with a primitive equation model to study the barotropic and baroclinic circulation of the Eastern Mediterranean.

In this study, we focus on global flow structure and properties, water mass formation processes, and seasonal variability of the circulation.

The following section is devoted to a description of the model, the bathymetry, the grid, the initial conditions, and the surface forcing. In section 3, the thermohaline circulation is discussed and background information is provided along with model results. Section 4 describes deep-water formation. Section 5 describes the near-surface circulation. In section 6 we offer a discussion and conclusions. Finally, the appendix provides further model calculations that inquire into the sensitivity of the surface flow to variations in surface forcing.

2. The ocean model

a. The governing equations

The ocean model is the Princeton ocean model, described in detail by Blumberg and Mellor (1987). It has been applied to coastal and estuarine bodies of water (Blumberg and Mellor 1983; Galperin and Mellor 1990a,b; Oey et al. 1985a,b,c), the Gulf Stream (Mellor and Ezer 1991), and many other oceanic regions. A description of the model code can be found in Mellor (1991a). It is a primitive equation model with a free surface, a split mode time step, and solves the following equations for the ocean velocity $U_i = (U, V, W)$, potential temperature θ, and salinity S:

$$\frac{\partial U_i}{\partial x_i} = 0 \tag{1}$$

$$\frac{\partial}{\partial t}(U, V) + \frac{\partial}{\partial x_i}[U_i(U, V)] + f(-V, U) = -\frac{1}{\rho_0}\left[\frac{\partial p}{\partial x}, \frac{\partial p}{\partial y}\right] + \frac{\partial}{\partial z}\left[K_M \frac{\partial}{\partial z}(U, V)\right] + (F_U, F_V) \tag{2}$$

$$\frac{\partial \theta}{\partial t} + \frac{\partial}{\partial x_i}(U_i\theta) = \frac{\partial}{\partial z}\left[K_H \frac{\partial \theta}{\partial z}\right] + F_\theta + \frac{\partial R}{\partial z} \tag{3}$$

$$\frac{\partial S}{\partial t} + \frac{\partial}{\partial x_i}(U_i S) = \frac{\partial}{\partial z}\left[K_H \frac{\partial S}{\partial z}\right] + F_S\,. \tag{4}$$

The vertical mixing coefficients K_M and K_H in (2)–(4) are calculated using the Mellor and Yamada (1982) turbulence closure scheme, whereas the horizontal diffusion terms (F_U, F_V), F_θ, and F_S in (2)–(4) are calculated using a Smagorinsky horizontal diffusion formulation (Mellor and Blumberg 1985). The term R in (3) is the portion of the shortwave radiation flux that penetrates the sea surface.

The hydrostatic approximation yields

$$\frac{p}{\rho_0} = g(\eta - z) + \int_z^\eta g\frac{\rho' - \rho_0}{\rho_0}\,dz'\,, \tag{5}$$

where $\eta(x, y)$ is the free surface elevation, ρ_0 is a reference density, and $\rho = \rho(\theta, S, p)$ is the density calculated by an adaptation of the UNESCO equation of state by Mellor (1991b) that uses potential temperature rather than in situ temperature as its argument.

b. The model grid

The model uses a bottom-following, sigma-coordinate system $\sigma = (z - \eta)/(H + \eta)$, where $H(x, y)$ is the bottom topography. The transformed equations can be found in the papers cited above. In the present study, the model has 16 vertical sigma levels (0.000, −0.003, −0.006, −0.012, −0.025, −0.050, −0.100, −0.200, −0.300, −0.400, −0.500, −0.600, −0.700, −0.800, −0.900, −1.000). The horizontal grid is the curvilinear orthogonal grid shown in Fig. 2a and contains 113 × 39 grid points. The grid resolution ranges from a minimum of 8–15 km in the Alboran Sea and Gibraltar region to a maximum of 50–60 km in the northernmost part of the basin. The time step was 24 min, and run time was 2.9 h per model year on a single Cray YMP-8 processor.

c. Bathymetry and initial conditions

The model bathymetry was obtained from the U.S. Navy bathymetric database DBDB5 by bilinear interpolation of the depth data onto the model grid. The resulting topography is illustrated in Fig. 2b and shows the major features of the basin's geometry including the islands of Sardinia, Corsica, Sicily, Mallorca, Crete, Cyprus, and Rhodes.

Figure 2c locates transects A, B, and C for depth–distance displays of the initial conditions and results from the tenth year of the calculations.

The model was initialized with annual climatological averages of temperature and salinity prepared by the National Institute for Oceanography and Fisheries at Alexandria (Egypt), using the NODC (National Oceanographic Data Center) and the WDC (World Data Center) databases. The annual averages are mapped on a 1/4° × 1/4° grid with 29 depth layers (0, 10, 20, 30, 50, 75, 100, 125, 150, 200, 250, 300, 400, 500, 600, 700, 800, 900, 1000, 1100, 1200, 1300, 1400, 1500, 2000, 2500, 3000, 3500, 4000 m). The grid points with missing data were filled by interpolation of the surrounding values. The surface temperature, salinity, and annual averages are shown in Fig. 3; cross-sectional plots on transect A are in Fig. 4.

d. Surface and bottom boundary conditions

The surface boundary conditions are surface heat flux, surface salinity flux, and wind stress. The monthly surface heat flux and wind stress averages were obtained by May (1982; P. W. May 1986, unpublished manuscript) on a 1° × 1° grid. The surface heat flux components are shortwave radiation Q_S, longwave radiation Q_l, sensible heat flux Q_h, and latent heat flux Q_e. The total heat flux Q_t is then given by

$$Q_t = Q_S + Q_l + Q_h + Q_e\,. \tag{6}$$

A part of (6), $Q_l + Q_h + Q_e$, plus a portion of the shortwave radiation is absorbed at the surface, where the boundary condition is

$$\left(K_H \frac{\partial \theta}{\partial z}\right)_{z=\eta} = (1 - \mathrm{Tr})Q_S + Q_l + Q_h + Q_e\,; \tag{7}$$

the remainder is directly added to the heat equation (3) as $\partial R/\partial z$, where

$$R = Q_S\,\mathrm{Tr}\exp(\lambda z)\,. \tag{8}$$

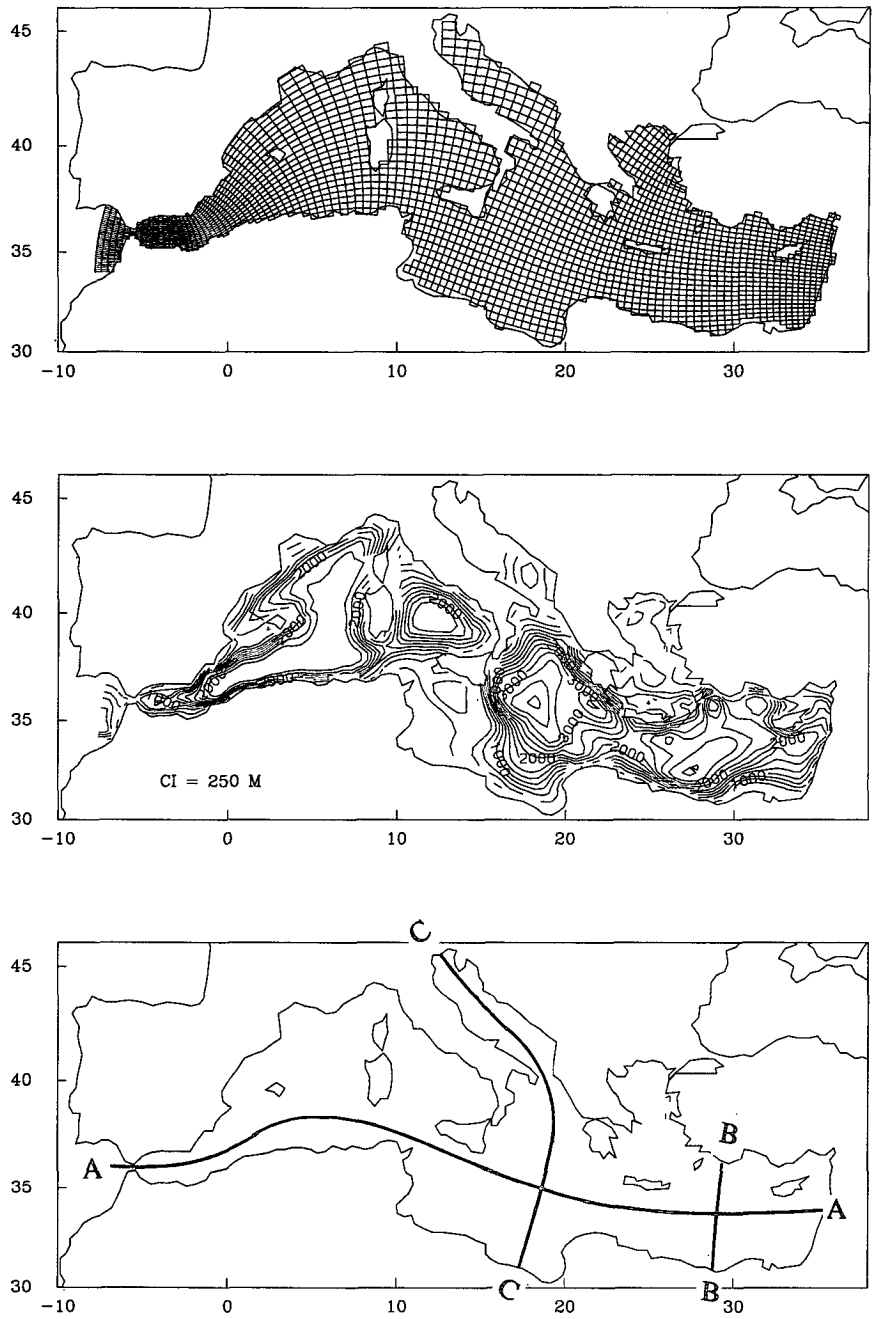

FIG. 2. (Upper) the model grid; (middle) the model bathymetry. The contour interval is 250 m. (Lower) transects for the presentation of model results.

The transmission coefficient Tr = 0.31 and the attenuation coefficient $\lambda = 0.042\ m^{-1}$ are chosen to fit Jerlov's (1976) tabulated attenuation functions for a "clear" water type.

The total heat flux fields for the months of February and August, calculated according to (6), are shown in Fig. 5. The February field shows a large cooling area over the Gulf of Lions (WMED), while the EMED is characterized by a zonal pattern with the largest negative values in the northern part of the basin (around Rhodes). In August, the heat flux is positive everywhere and the minimal values are again found in the northern Balearic Basin and in the Rhodes region.

The monthly evaporation rate E was calculated from May's (1982) latent heat flux data according to

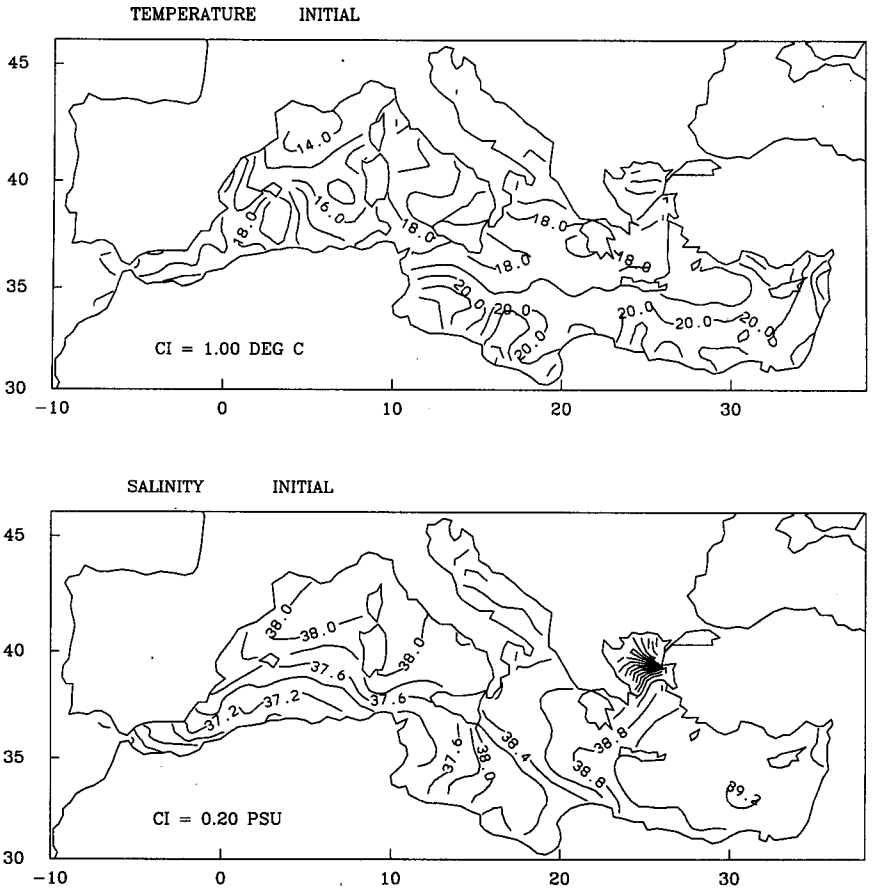

FIG. 3. Annually averaged hydrological climatologies (model initial conditions). (Upper) surface temperature; the contour interval is 1°C. (Lower) surface salinity; the contour interval is 0.1 psu.

$$E = \frac{Q_e}{L_v}, \tag{9}$$

where L_v is the latent heat of condensation. The monthly precipitation rate (P) was obtained from Jaeger (1976), whose data are mapped on a 5° × 2.5° grid. Finally, the fresh water surface flux W_S was calculated according to

$$W_S = E - P, \tag{10}$$

and the surface boundary condition for salinity is

$$\left(K_H \frac{\partial S}{\partial z}\right)_{z=\eta} = W_S S_{z=\eta}. \tag{11}$$

The calculated total annual fresh water loss is 0.92 m yr^{-1}, a value that agrees reasonably well with the results of many budget calculations. The monthly averages range between a minimum of 3.6 cm mo^{-1} in May and a maximum of 10.5 cm mo^{-1} in August. The W_S fields for the months of February and August are shown in Fig. 6 and are very similar to the total heat flux fields of Fig. 5 since the latent heat flux component dominates both fields.

The wind stress fields for the same months are illustrated in Fig. 7. One sees evidence of the gaps between the mountain ranges bordering the northern Mediterranean coasts. The most prominent winter feature characterizing the WMED is the occurrence of a strong northerly wind, the Mistral, blowing from the Rhône River Valley through the opening between the Alps and the Pyrenees. In the EMED, the wind stress is mostly zonal. In the northern Adriatic there occurs an easterly wind, the Bora, blowing over the sea from the opening between the Alps and the Dynaric Alps; this wind can be very strong but it is not as frequent as the Mistral and, climatologically, it results in only a slightly larger stress. In August, the Mistral still affects the WMED although with reduced stress. In the EMED, the dominant winds are the Etesians, blowing from the opening between the Balkans and the Anatolian Mountains over the Levantine Sea with a cyclonic curvature. The wind stress direction over the Adriatic and the Ionian Seas is mainly meridional.

All the surface boundary conditions were applied to the model by interpolating linearly between adjacent monthly values.

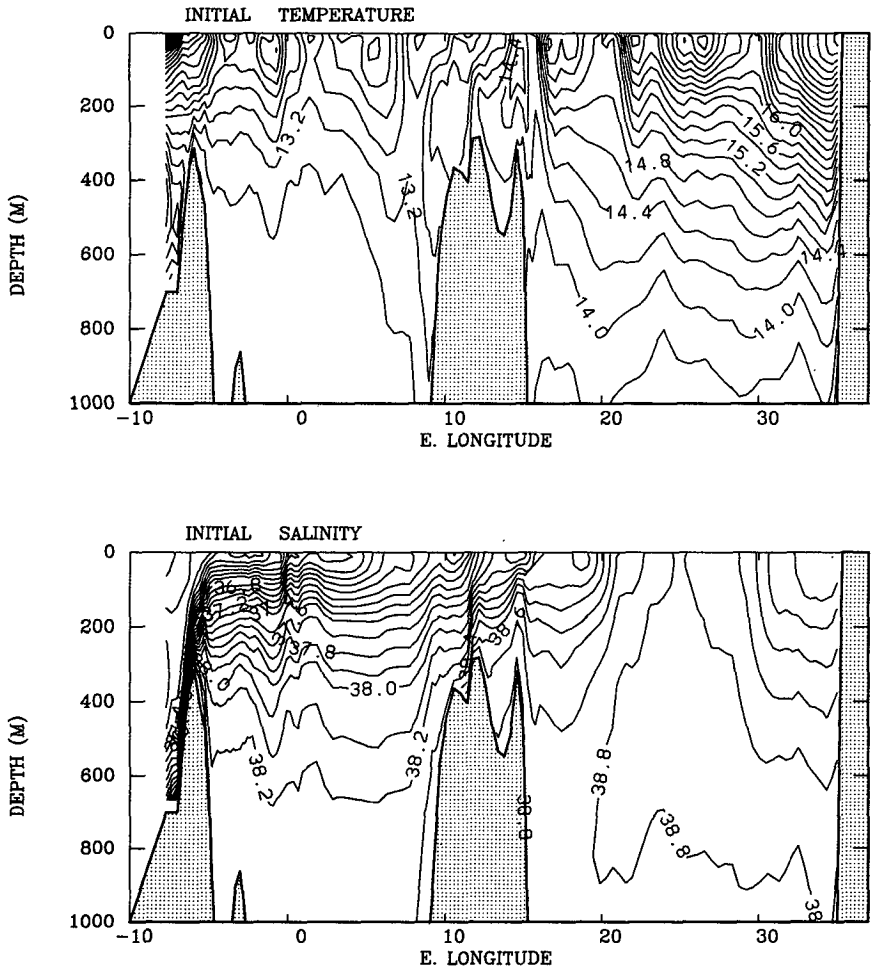

FIG. 4. Annually averaged hydrological climatologies (model initial conditions) on cross section A. (Upper) surface temperature; the contour interval is 0.2°C. (Lower) surface salinity; the contour interval is 0.1 psu.

At the bottom, adiabatic boundary conditions are applied to temperature and salinity. For velocity, a quadratic drag coefficient of 0.01 is used.

e. *Lateral boundary conditions*

The model has one open boundary in the Atlantic Ocean about 200 km west of the Strait of Gibraltar where the internal normal velocities are governed by a Sommerfeld radiation condition; constant elevation is specified as the external open boundary condition. Temperature, salinity, and tangential velocities are upwinded on the boundary; when the flow is into the model domain temperature and salinity are prescribed from the observed climatology; tangential velocity is null.

The annually averaged freshwater river discharge for the Rhône and Ebro Rivers (1700 and 550 $m^3 s^{-1}$) in the WMED, the Po River in the Adriatic Sea (1550 $m^3 s^{-1}$), and the Black Sea (6000 $m^3 s^{-1}$) were added to the model. Additional discharge due to the remainder of the rivers (6000 $m^3 s^{-1}$) was uniformly subtracted from W_S. The average values are those reported in UNEP (1984) and by Harzallah et al. (1993) who cite a number of sources.

3. The thermohaline circulation of the Mediterranean

a. *Background information*

The circulation and hydrography of the Mediterranean Sea waters are driven by the net fresh water loss and heat loss to the atmosphere and the exchange of salinity and heat through the Straits of Gibraltar. The loss by evaporation exceeds the input by precipitation and river runoff and Black Sea exchange. The May–Jaeger freshwater deficit amounts to about 73 000 $m^3 s^{-1}$, corresponding to an average fresh water removal of 0.92 m yr^{-1} over the entire sea surface.

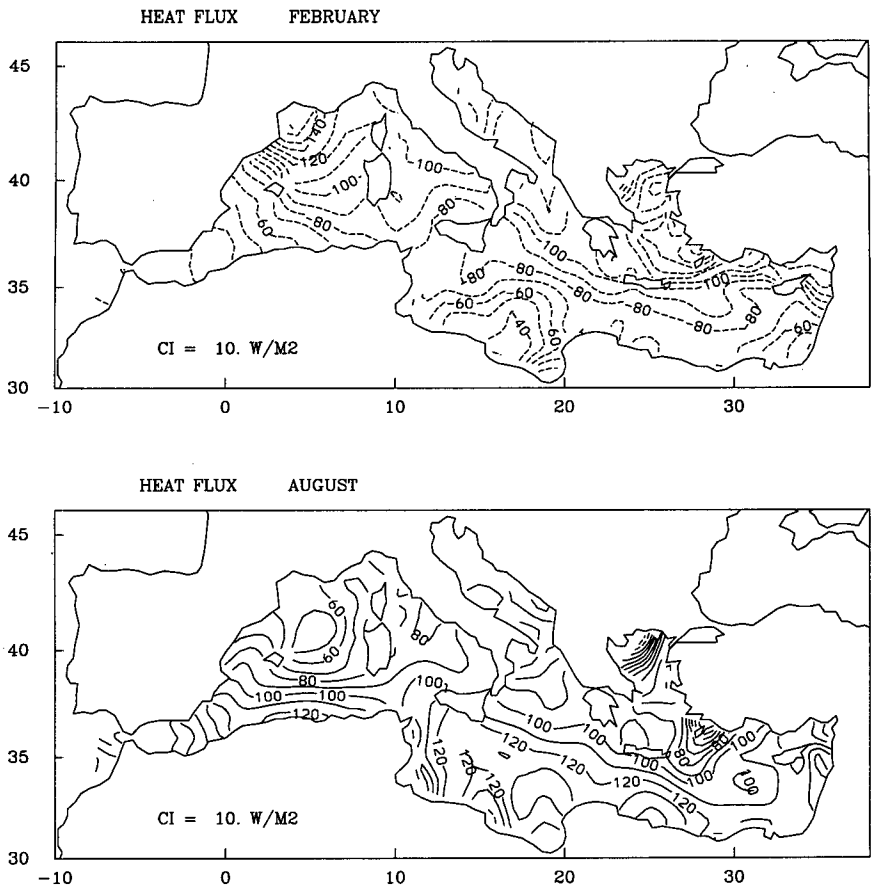

FIG. 5. Total surface heat flux. (Upper) February; (lower) August; the contour interval is 10 W m^{-2}.

The existence of the two counterflows in the Strait of Gibraltar requires a basin transformation to link the inflowing Atlantic Water with the outflowing Levantine Intermediate Water (LIW); a vertical distribution is schematized in Fig. 8. The surface waters, the Modified Atlantic Water (MAW), flowing into the Mediterranean are subject to evaporation and mixing with the underlying waters, causing a progressive increase of the salinity; the surface value increases from 36.25 psu in the Gibraltar area to 37.25 psu in the Strait of Sicily and to values higher than 38.50 psu in the Levantine Sea. Its west to east path across the Mediterranean can be tracked by a subsurface salinity minimum (Lacombe and Tchernia 1960), representing the signature of their Atlantic origin, which progressively deepens from 20 to 50 m.

The LIW depth range is 300–700 m in the WMED and 200–400 m in the EMED. LIW is the result of winter convection processes in the EMED occurring in the Rhodes–Cyprus area, and probably in other sectors of the Levantine Sea in winter (Morcos 1972). At its source, LIW has a salinity of about 39.10 psu and spreads to the whole Mediterranean (S = 38.70 psu at the Strait of Sicily), reaching Gibraltar where it forms the Mediterranean outflow into the Atlantic Ocean.

A classical and informative, albeit approximate, analysis of the salinity and heat exchange is obtained by balancing mass flux and salt flux using a two-layer model. Neglecting river and Black Sea exchange, one obtains

$$Q_1(S_1 - S_2) - Q_{ev}S_2 = 0 \qquad (12)$$

and also $Q_2 = Q_1 - Q_{ev}$. Here Q_1 and Q_2 are the volumetric inflow and outflow rates at the Strait of Gibraltar; Q_{ev} is the net evaporation–precipitation, surface fresh water exchange rate; and S_1 and S_2 are the inflow and outflow salinities. From Figs. 4 or 8, we use $S_2 - S_1 \approx 2$ psu and $S_2 = 38$ psu so that, with $Q_{ev} = 73\,000$ m^3 s^{-1} = 0.073 Sv, we obtain $Q_1 \approx 1.39$ Sv and therefore $Q_2 \approx 1.32$ Sv $\approx Q_1$.

The corresponding heat balance yields

$$\rho C_p Q_1(\theta_1 - \theta_2) + H_S = 0\,, \qquad (13)$$

where H_S is the surface heat transport. From Fig. 4 a rough estimate of the annual average temperature dif-

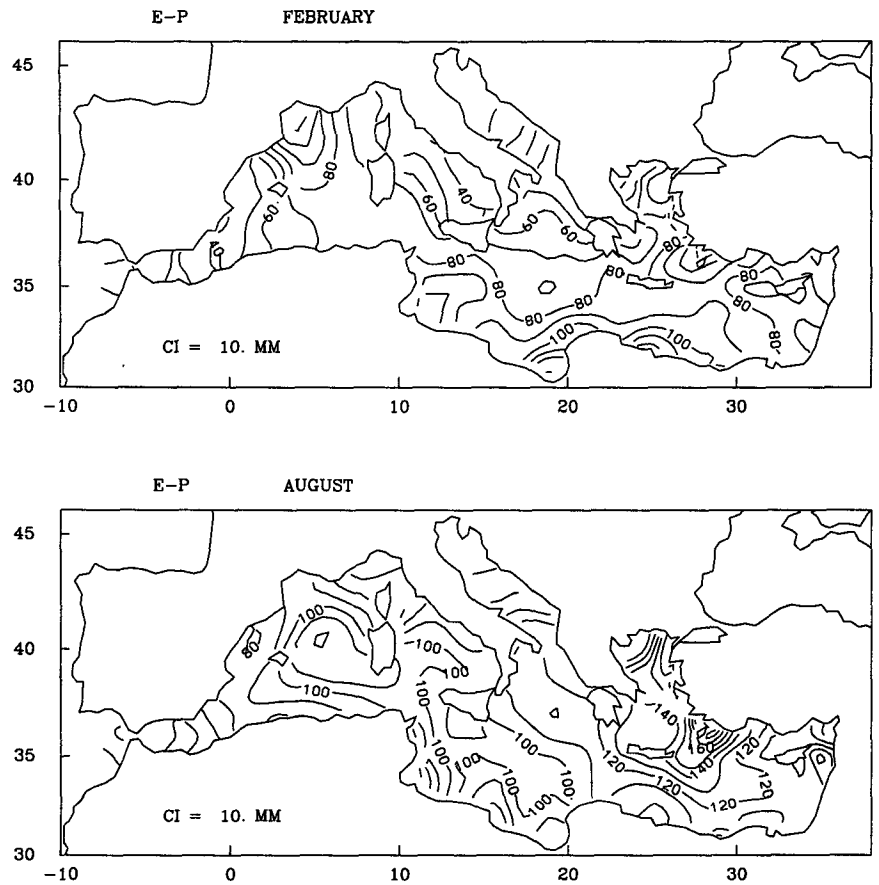

FIG. 6. Surface fresh water flux. (Upper) February; (lower) August; the contour interval is 10 mm.

ference $\theta_2 - \theta_1$ is about 2.5°C; therefore (13) yields a heat transport $H_S = -1.38 \times 10^{13}$ W, or an area averaged flux of -5.6 W m^{-2} *out* of the basin. Note that this balance, although approximate, places some constraint on surface heat flux evaluations from surface ship data and bulk heat flux and radiation formulas. Garrett et al. (1993) review these calculations in considerable detail and conclude that, using generally accepted bulk formulas and empirical constants, one obtains surface heat flow *into* the basin, which, in view of (13) and other surveys in the Strait, is not possible; they estimate $H_s/A_M = -7 \pm 3$ W m^{-2}. Estimates of Q_{ev} are also uncertain, a matter that has been discussed by Gilman and Garrett (1994) and Harzallah et al. (1993). We shall return to these budget considerations in the context of our model simulations. The model will be forced by surface fluxes, whose integrals are approximated by $Q_{ev}S_2$ and $-H_s$ in (12) and (13). If the strait fluxes produced by the model (plus fluxes represented by small rivers and the Black Sea) are not in balance, then the tendency of the seasonal and volume integrated temperature and salinity will be nonzero.

b. *Model results*

The immediate challenge for a numerical model is to replicate the Gibraltar/MAW/LIW system, to determine whether or not the model flow structure accords with reality.

The model was run for 10 years. During this time we maintained a continuous and exact accounting of the monthly and yearly temperature and salinity budgets in the form

$$V_M \frac{\delta \bar{P}}{\delta t} = G_{P\text{surf}} + G_{P\text{gib}} + G_{P\text{riv}}, \qquad (14)$$

where the basin volume $V_M = 3.77 \times 10^{15}$ m^3; P is either temperature, multiplied by $\rho_0 C_p$, or salinity, volumetrically averaged throughout the basin. The G_P are heat or salinity transports that are obtained by numerical integration of model fluxes. Thus, $G_{P\text{surf}}$ is the transport through the basin surface, $G_{P\text{gib}}$ is the transport through the Strait of Gibraltar, and $G_{P\text{riv}}$ is the river transport including the Black Sea. The overbar on P represents a volumetric average and the difference

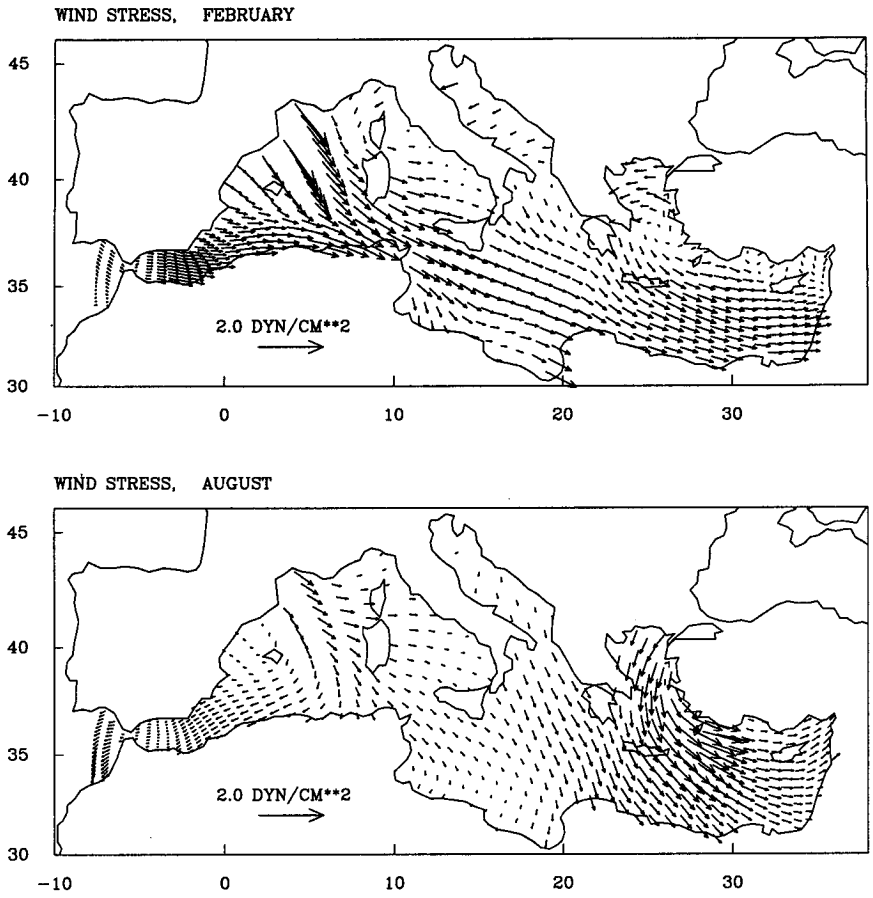

FIG. 7. Wind Stress: (upper) February; (lower) August. Units are dynes per square centimeter. Vectors are plotted at every other grid point.

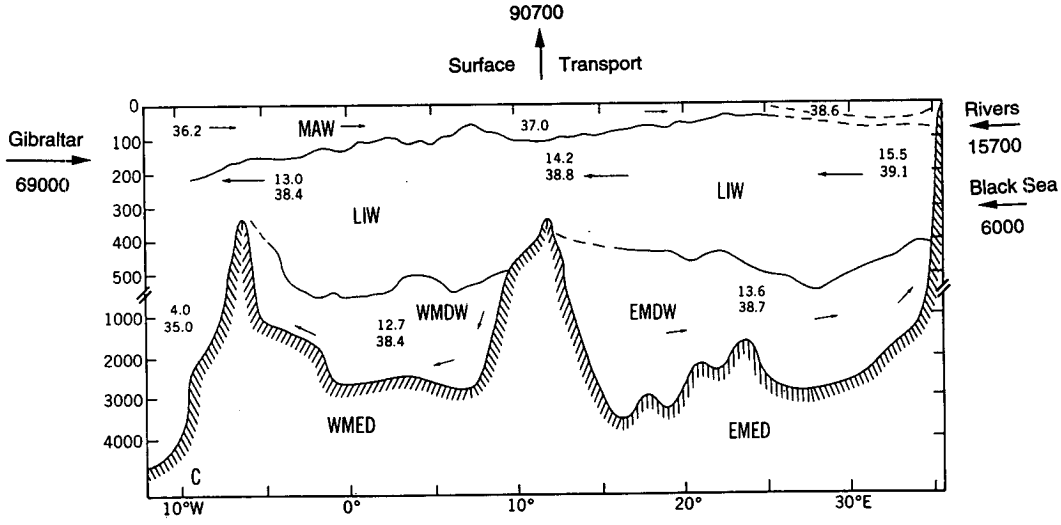

FIG. 8. Schematic of the Mediterranean Sea water masses vertical distribution (adapted from Hopkins 1985). The model-derived equivalent freshwater budget is also shown. The units are $m^3 s^{-1}$. The value 90 700 $m^3 s^{-1}$ is equal to an area-averaged freshwater removal of 1.13 m yr^{-1}.

operator δ is a yearly difference. The river heat transport $G_{\theta\text{riv}}$ has been neglected.

Although the May heat flux is in error by a fairly small amount, the sign of the net temporal and spatial average is incorrect. The average heat flux was +2.5 W m^{-2} whereas, for the first two years, the model-derived annually and cross-sectionally averaged heat flux across the Strait of Gibraltar $G_{\theta\text{gib}}$, when divided by the basin surface area $A_M = 2.48 \times 10^{12}$ m^2, was −4.5 W m^{-2}, a value in fair agreement with the simple two layer estimate and the estimate of Garrett et al. (1993). We have therefore adjusted the surface heat flux by subtracting a constant value so that surface heat flux balanced the Gibraltar flux. For the remaining eight years, the annually and volumetrically averaged temperature $\bar{\theta}$ was virtually invariant.

The surface salinity flux is more uncertain. A key question is whether or not the model will produce a reasonable value of $G_{S\text{gib}}$, the yearly averaged salinity transport through the Strait of Gibralter. This quantity was numerically well behaved; it decreased exponentially from the value -3.08×10^6 psu m^3 s^{-1} for year 2 to the value -2.65×10^6 for year 10 and, in the intervening years, very closely followed the curve fit

$$G_{S\text{gib}} = G_\infty + (G_0 - G_\infty)\exp(-t/T), \quad (15)$$

where $G_\infty = -2.62 \times 10^6$ psu m^3 s^{-1} and G_0 is the year 2 value and t is measured from year 2; we also find that $T = 2.78$ yr. Thus, most of the adjustment of $G_{S\text{gib}}$ occurred in the first few years.

During the first five years, the annual and basin averaged salinity decreased from 38.596 to 38.565 psu. Thereafter, the surface salinity flux was amended so that the average salinity was virtually constant. The final flux values (using the value G_∞ for salinity transport through the strait) that render invariant the annually and spatially averaged temperature and salinity are summarized in Fig. 8. The surface freshwater transport essentially *required* by the model and the initial conditions is 90 700 m^3 s^{-1}, or 1.13 m yr^{-1}, which is on the high end of estimates by several researchers but is not improbable. Salinity transports can, to good approximation, be converted to equivalent fresh water volumetric flows upon division by 38 psu.

Henceforth, all results are extracted from the tenth year of the model run.

Figures 9a,b exhibit winter and summer temperature and salinity plots on cross section A, the main backbone of the Mediterranean. (Since the plots are quite compact, they have been smoothed slightly to enhance clarity.) Also shown are plots of the streamfunction, obtained by integrating the east–west velocity horizontally and vertically on the curvilinear coordinate approximately normal to cross section A; see Fig. 2a. (The depth is the *maximum* depth on the normal coordinate and does not equal the depths on the temperature and salinity sections.) At Gibraltar, there is an inflow of 1.32 Sv at the surface and an equal return flow in the bottom-most layers; the flow is quite invariant in both summer and winter. Above 300 or 400 m in the WMED and EMED, there is a pronounced seasonal signal in both temperature and salinity; below, there is no seasonal signal.

The salinity distribution in Fig. 9b shows that the model is successful in reproducing and maintaining a well-known feature of the Mediterranean thermohaline structure, the summer development of a subsurface salinity minimum marking the path of the MAW flowing into the basin, which is modified by the surface warming and freshwater losses. The salinity minimum is clearly defined in the WMED at depths of about 30–50 m; it extends throughout the whole basin, reaching the Strait of Sicily, developing in the EMED at a depth of about 50 m as far as the Cretan Passage, and vanishing into the Levantine Sea. In both basins the salinity minimum is not developed in winter and appears only during the summer seasons throughout the entire integration time of the model.

The 10-yr temperature and salinity fields in Fig. 9c do not generally differ from the initial conditions in Fig. 4. The largest error is 0.2–0.4 psu in the 200–600 m range in the WMED.

Lascoartos et al. (1993) define LIW "core" characteristics corresponding to depths of 150 to 400 m, temperatures in the range 15°–16°C, and salinities in the range 38.95–39.05 psu although they cite researchers who ascribe a wider range of values. These properties may be seen in Figs. 9a–c with a center slightly west of 30°E. The north-central sector of the Levantine Sea, the Rhodes–Cyprus area, is a well-investigated LIW source area (see for instance, Ovchinnikov 1984) so that, in Fig. 10a, we show the winter distribution of potential temperature, salinity, and turbulence kinetic energy along the meridional cross section B crossing the Rhodes–Cyprus region and the Levantine Sea. One can see LIW core water intersecting the surface. The turbulence and concomitant mixing is a manifestation of the fact that the static stability $\partial\rho/\partial z - c^{-2}\partial p/\partial z$, where c is the speed of sound, is positive in the upper 200 m. This situation is of course reversed in the summer. The "bull's eye" around 32°N is a local, advectively induced instability. The distribution of temperature shows some doming of the isotherms in the center of the section determined by the Rhodes cyclonic gyre (Anati 1984). In August, Fig. 10b shows a Rhodes gyre that has migrated slightly to the north.

Lascoartes et al. (1993) used an array of one-dimensional, model mixed layers and a parameterization of horizontal advection to estimate LIW formation. By assuming that all water formed in the mixed layer with LIW core characteristics was subducted into the LIW, they estimated the formation rated at 1.0 Sv; they state that this value may be overestimated. Figure 9 indicates about 0.6 Sv of LIW water exiting the Strait of Sicily. However, unlike the very narrow Strait of Gibraltar (two north–south grid points), there is considerable

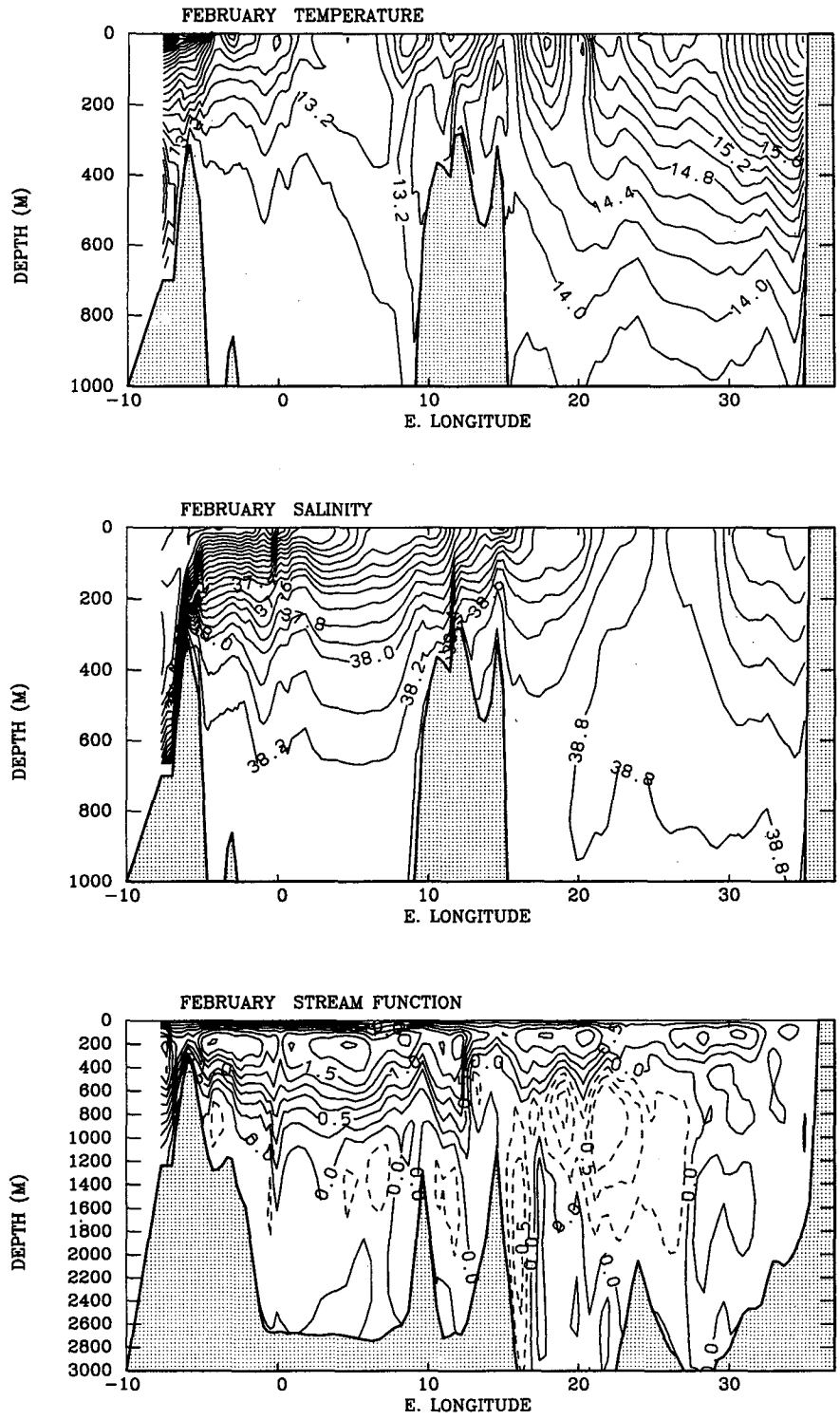

FIG. 9. (a) Model properties for February on cross section A. (Upper) temperature; the contour interval is 0.2°C. (Middle) salinity; the contour interval is 0.1 psu. (Lower) the streamfunction; the contour interval is 0.25 Sv.

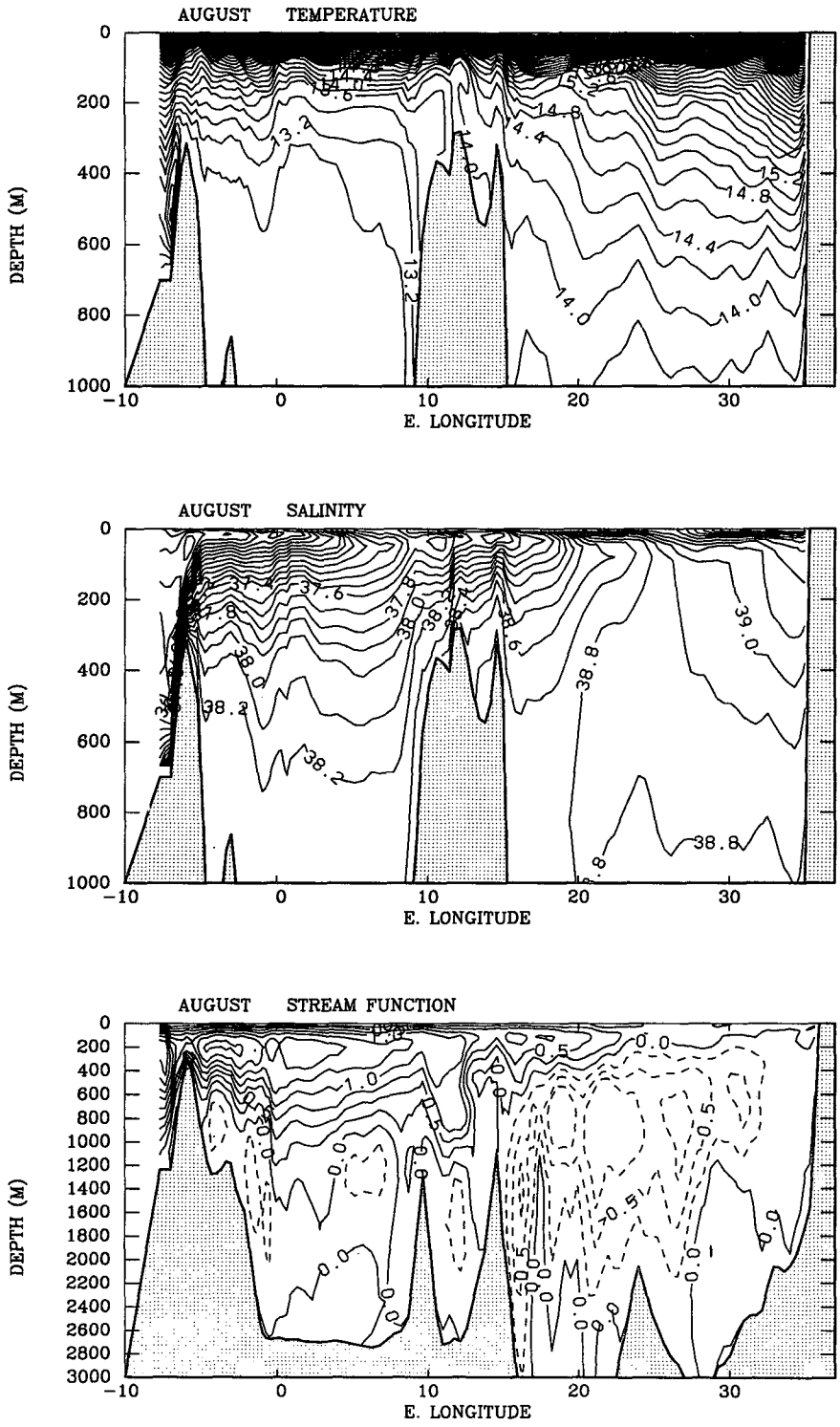

FIG. 9. (*Continued*) (b) Model properties for August on cross section A. (Upper) temperature; the contour interval is 0.2°C. (Middle) salinity; the contour interval is 0.1 psu. (Lower) the stream-function; the contour interval is 0.25 Sv.

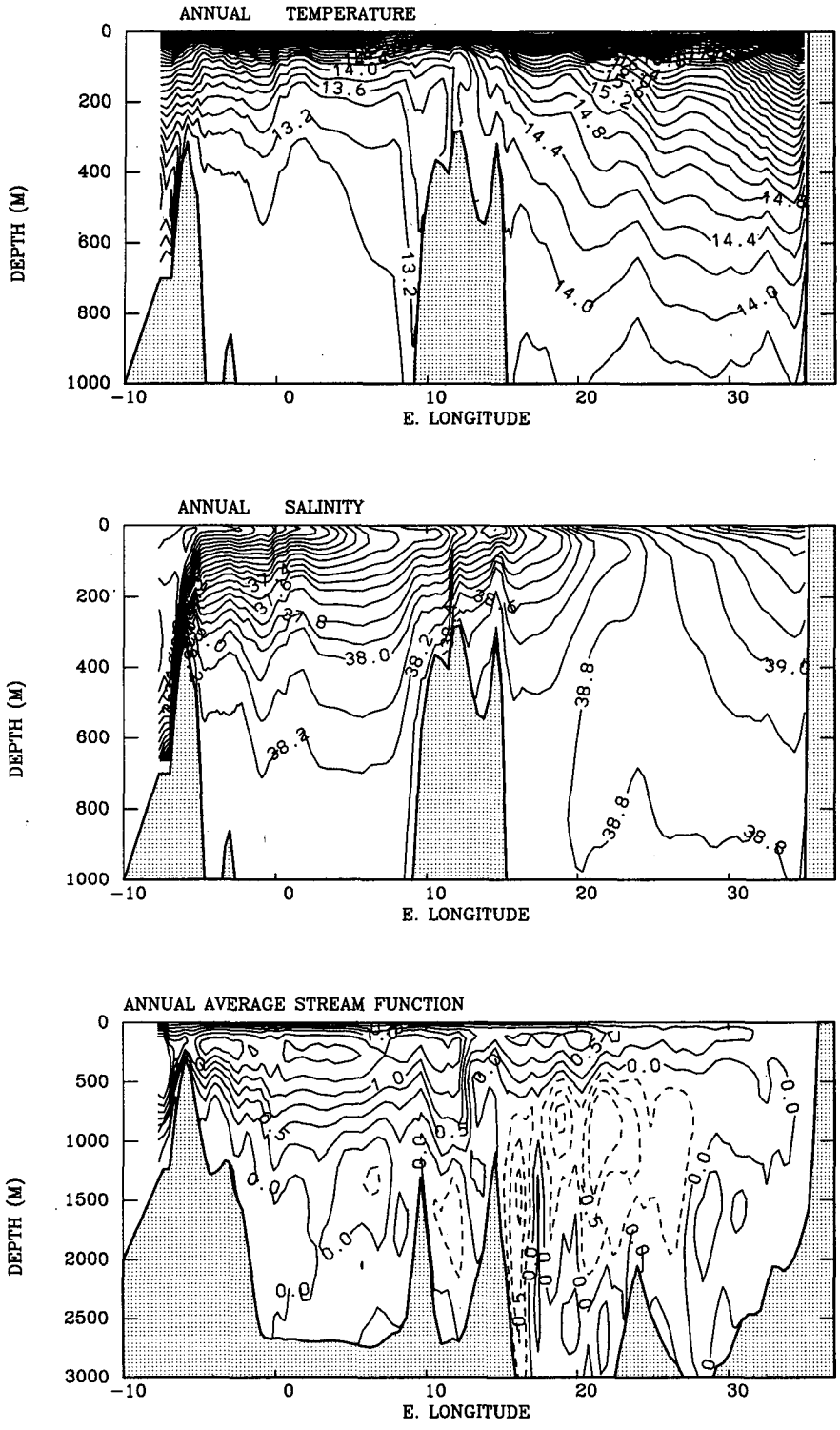

FIG. 9. (*Continued*) (c) Model properties for the annual average on cross section A. (Upper) temperature; the contour interval is 0.2°C. (Middle) salinity; the contour interval is 0.1 psu. (Lower) the streamfunction; the contour interval is 0.25 Sv.

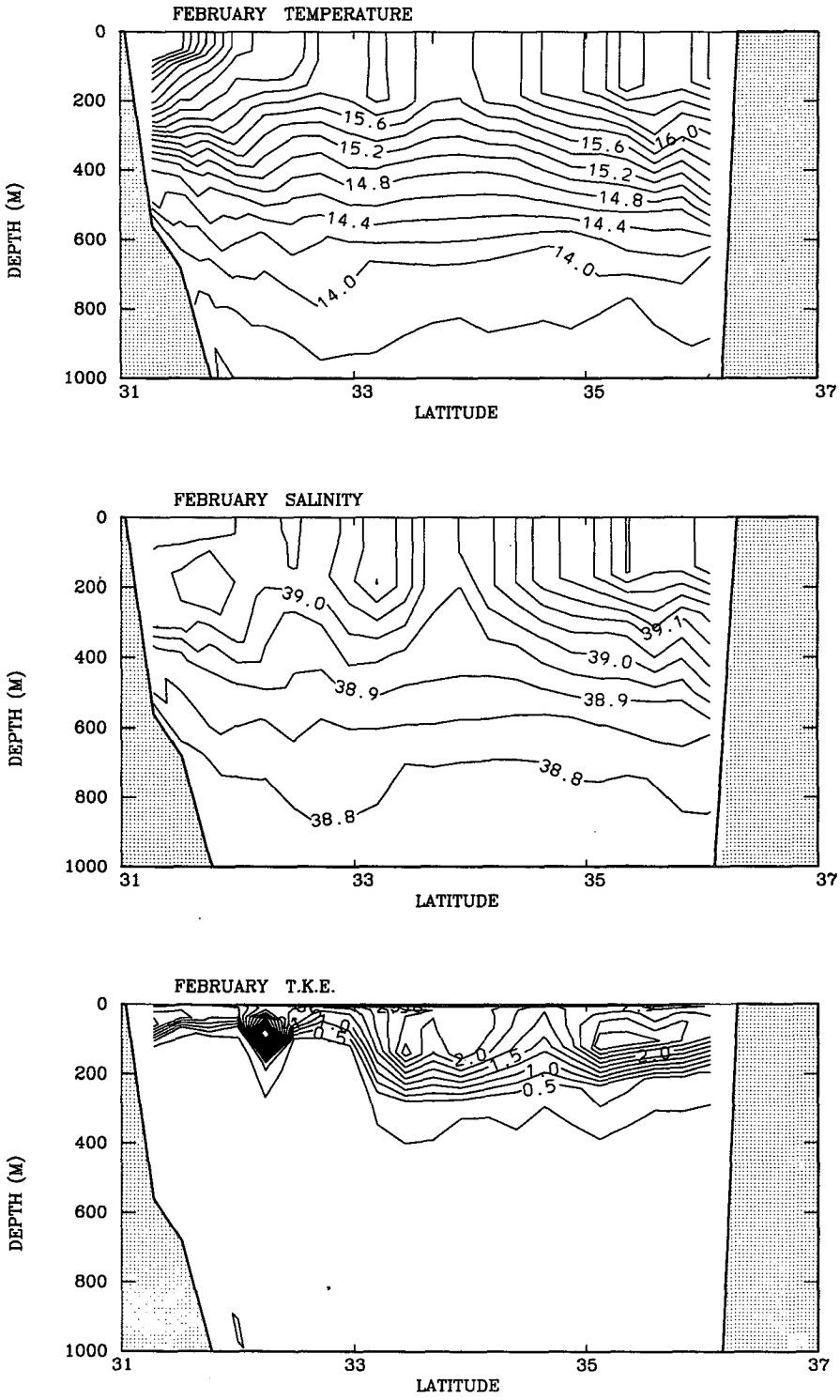

FIG. 10. (a) Model properties for February on cross section B. (Upper) temperature; the contour interval is 0.2°C. (Middle) salinity; the contour interval is 0.05 psu. (Lower) turbulence kinetic energy; the contour interval is 0.25×10^{-4} m^2 s^{-2}.

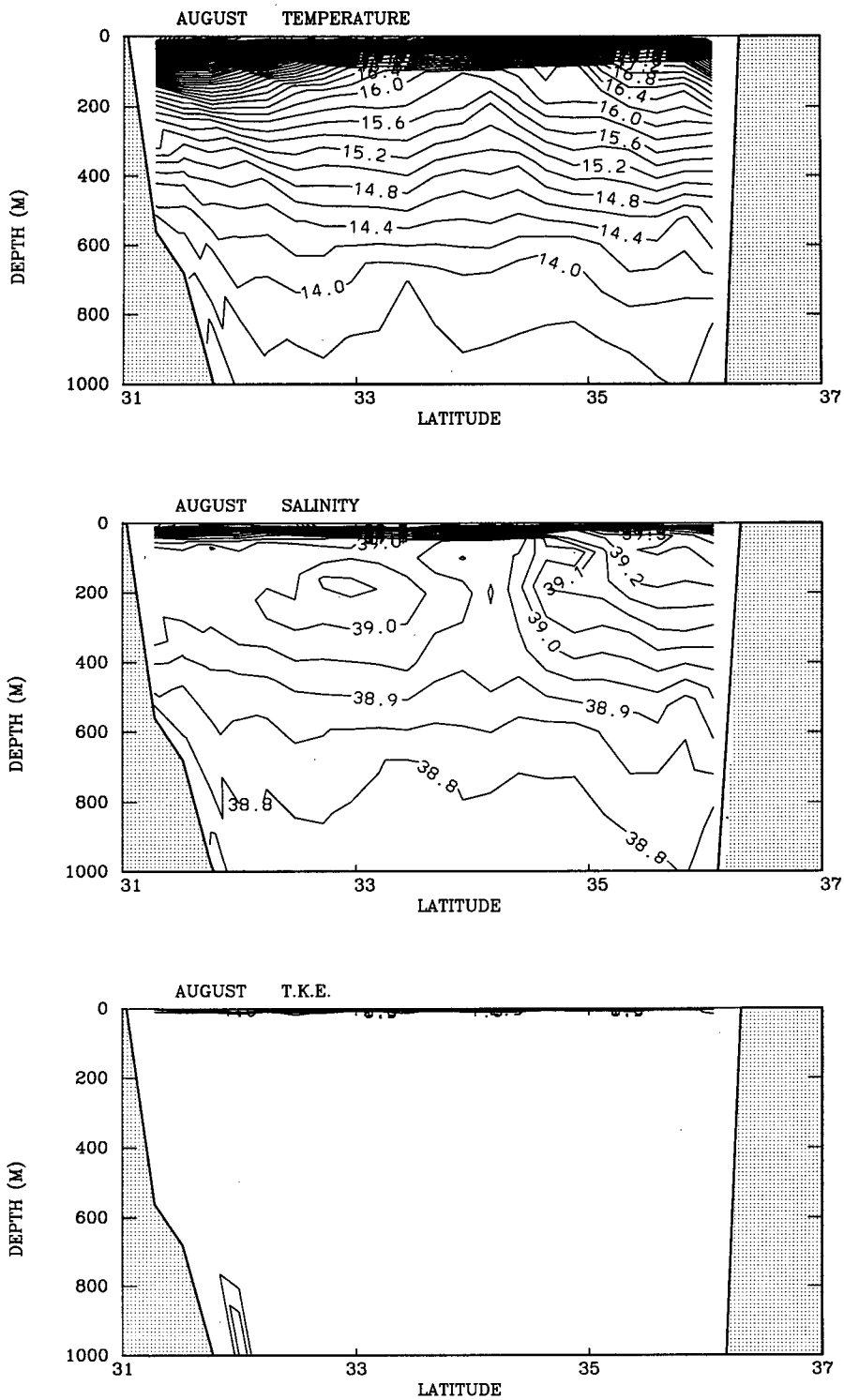

FIG. 10. (*Continued*) (b) Model properties for August on cross section B. (Upper) temperature; the contour interval is 0.2°C. (Middle) salinity; the contour interval is 0.05 psu. (Lower) turbulence kinetic energy; the contour interval is 0.25×10^{-4} m^2 s^{-2}.

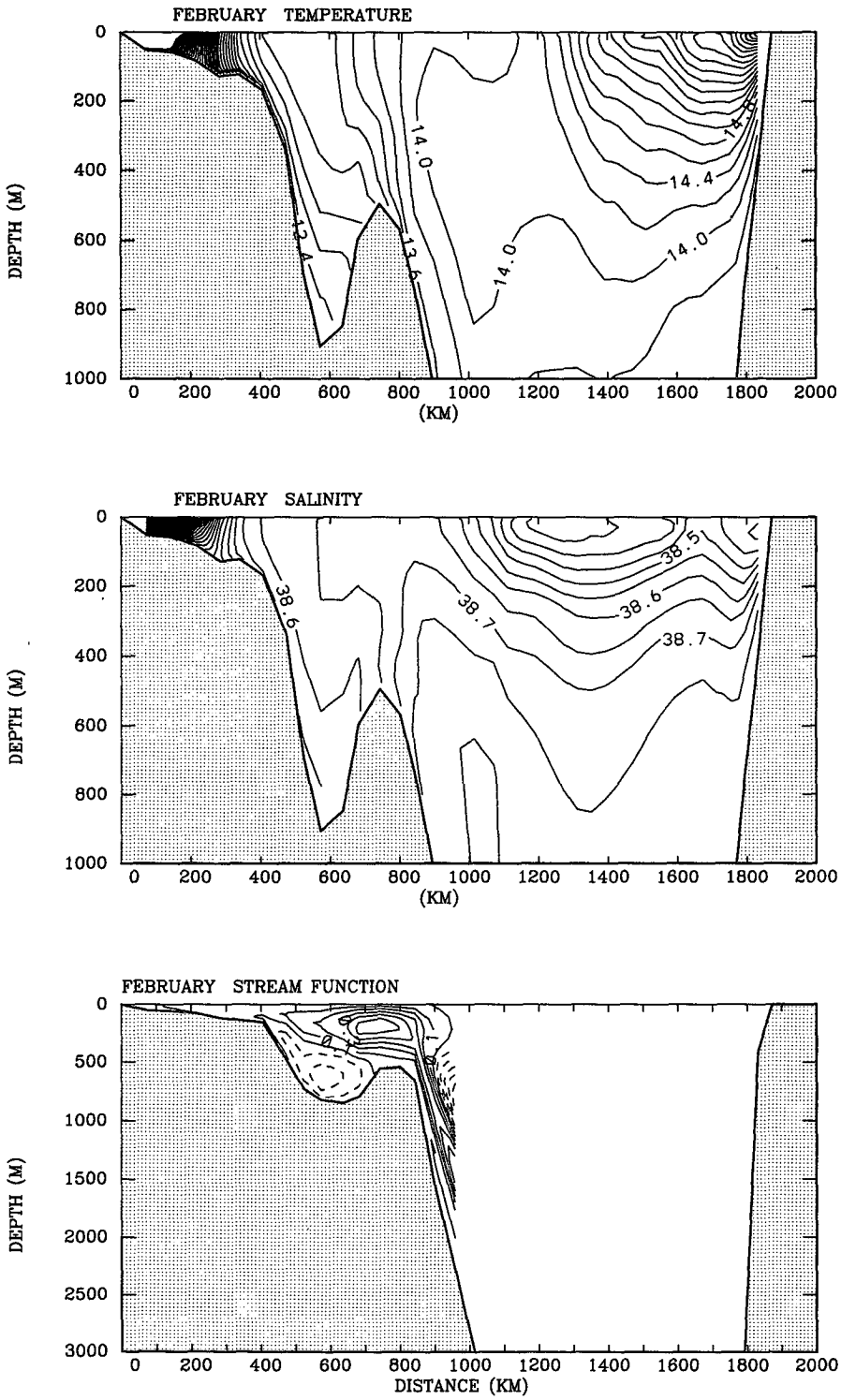

FIG. 11. (a) Model properties for February on cross section C. (Upper) temperature; the contour interval is 0.2°C. (Middle) salinity; the contour interval is 0.05 psu. (Lower) streamfunction; the contour interval is 0.1 Sv.

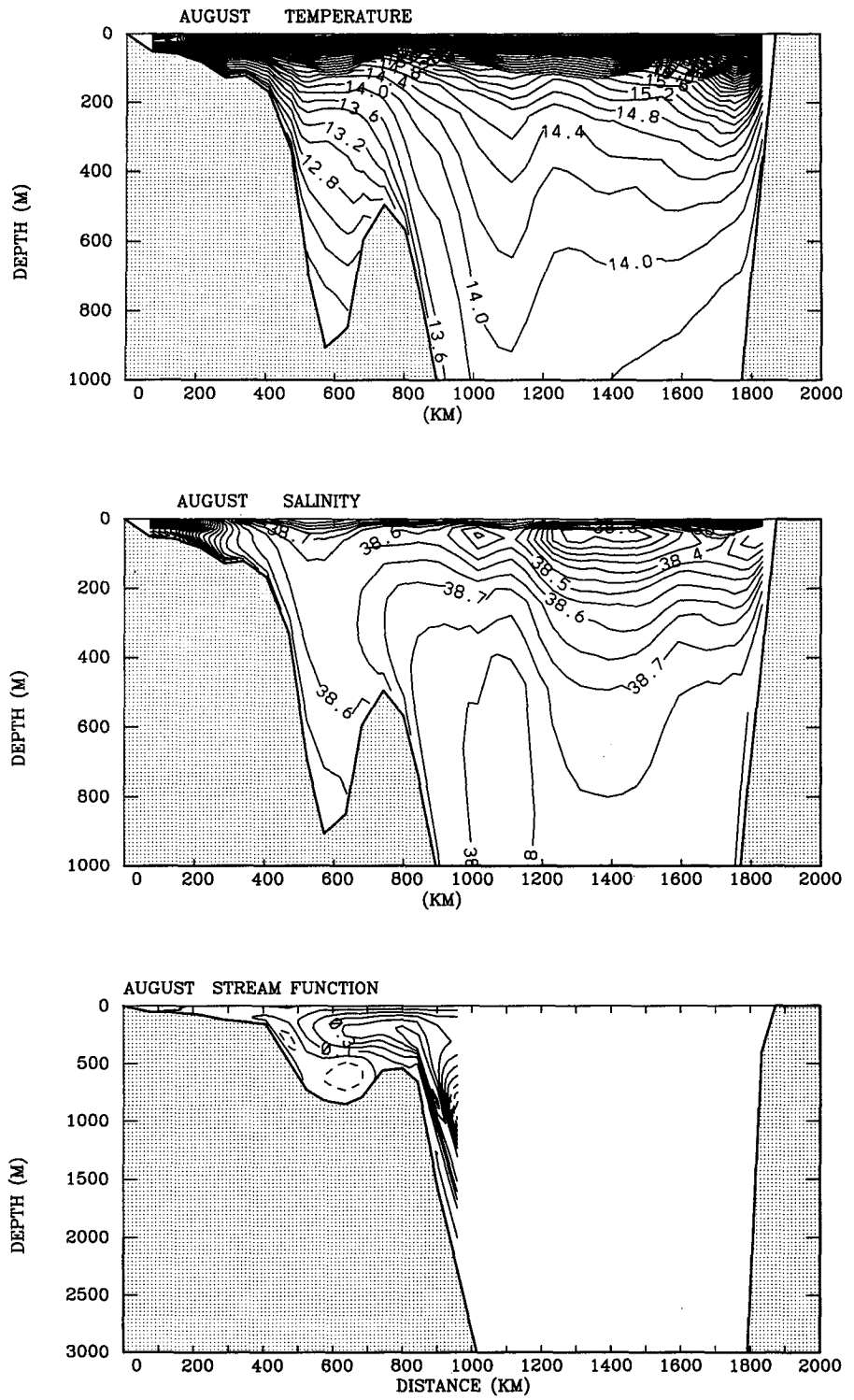

FIG. 11. (*Continued*) (b) Model properties for August on cross section C. (Upper) temperature; the contour interval is 0.2°C. (Middle) salinity; the contour interval is 0.05 psu. (Lower) streamfunction; the contour interval is 0.1 Sv.

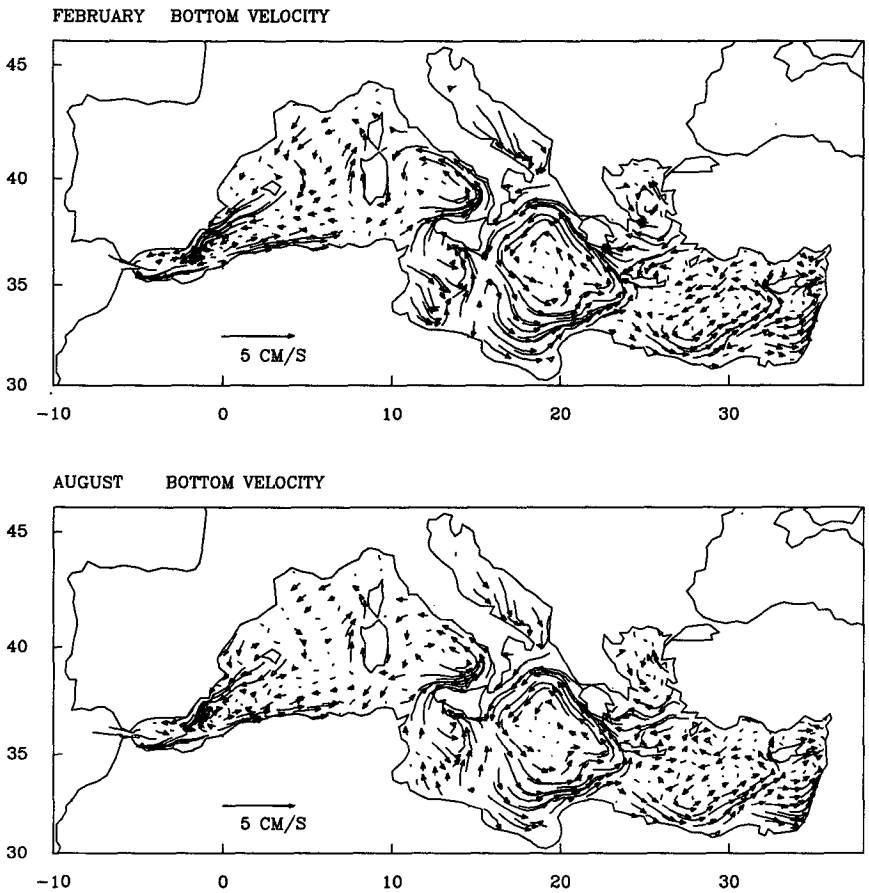

FIG. 12. The flow in the bottom-most sigma layer shown as Eulerian velocity trajectories corresponding to a particle trajectory (if the flow were steady) of 90 days. Although a fairly complicated diagram, when coordinated with topography in Fig. 2, one can see that the downwelling in the deeper water depicted in Fig. 11 occurs in the western borders of the Adriatic and the northwestern borders of the Ionian, whereas the upwelling in somewhat shallower water occurs in the eastern portions.

horizontal variability (not shown) in the Strait of Sicily, which is information lost in forming the zonally averaged streamfunction.

The streamfunction plots of Fig. 9 also show that, in the EMED below the MAW/LIW open cell of circulation, there are multiple closed cells of circulation encompassing the whole basin. Downwelling occurs in the Ionian Sea, while upwelling is present both in the Ionian and in the Levantine Sea. This kind of thermohaline circulation of the EMED resembles very closely the scheme proposed by the POEM Group (1992) on the basis of passive tracer distributions. Further insight on the origin of the ascending and descending branches of the thermohaline cell is offered in the section 4.

4. Deep-water formation

a. Background information

The deep-water formation areas of the WMED and of the EMED are geographically separate and the deep-water interface with the LIW is deeper than the sill depth of the Straits of Sicily, preventing exchange between the water masses.

The source of the eastern Mediterranean deep waters is the Adriatic Sea (Pollak 1951), where a water mass around $\theta = 13.60°C$ and $S = 38.70$ psu is formed in winter and spreads to the whole EMED deep basin. The traditional interpretation of the deep-water formation in the Adriatic Sea assigns a key role to the cooling and evaporative processes acting on the shelf waters of the northern Adriatic, causing their sinking along the continental slope. However, Ovchinnikov et al. (1987) observed a MEDOC-like deep-water formation in the southern Adriatic producing dense waters flowing into the Ionian Sea over the Otranto Sill, while the dense water formed in the northern Adriatic were not involved in the exchange.

The source of the Western Mediterranean deep water is located in the Gulf of Lions area, and the water mass formation, the so-called MEDOC deep-water forma-

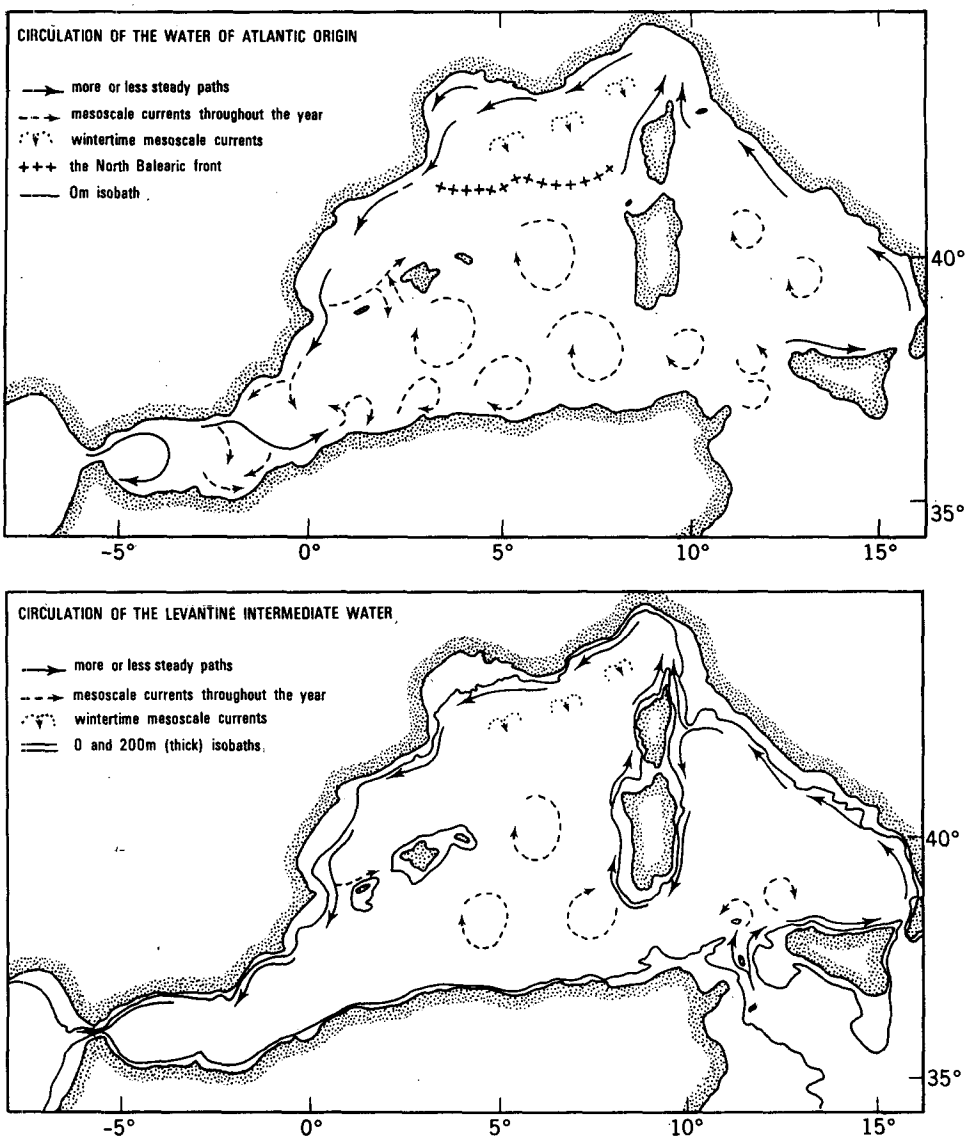

FIG. 13. (a) Schematic of the WMED circulation. (Upper) MAW circulation. (Lower) LIW circulation (adapted from Millot 1987a).

tion, takes place in winter (MEDOC Group 1969; Sankey 1973; Leaman and Schott 1991). There, intensive convective movements occur under the influence of cold and dry winds, causing the sinking and mixing of the relatively cold and salty surface waters to depths of about 1200–1500 m. The resulting water mass has a potential temperature θ of about 12.70°C and a salinity of 38.40 psu. This water mass can enter the Mediterranean outflow at Gibraltar without mixing with the LIW (Kinder and Parrilla 1987).

b. *Model results*

Potential temperature, salinity, and streamfunction (derived from normal velocities integrated horizontally normal to cross section C) are contoured in Figs. 11a,b, for cross section C, which crosses the Adriatic Basin from the Gulf of Venice to the Strait of Otranto and continues to the Gulf of Sirte. These figures should be coordinated with the flow field of the deepest sigma level in Fig. 12 and the topography in Fig. 2. One clearly observes the creation of dense water over the shallow northern shelf and in the southern Adriatic. The water mass produced in winter (Fig. 11a) flows south along the bottom (Artegiani and Salusti 1987) and then plunges into the deep abyss. The time of travel is of the order of a half year. The downwelling in the deepest water in Fig. 11 may also be identified with the flow along the western portions of the Adriatic and Ionian Seas in Fig. 12 as it slides into the deeper southern

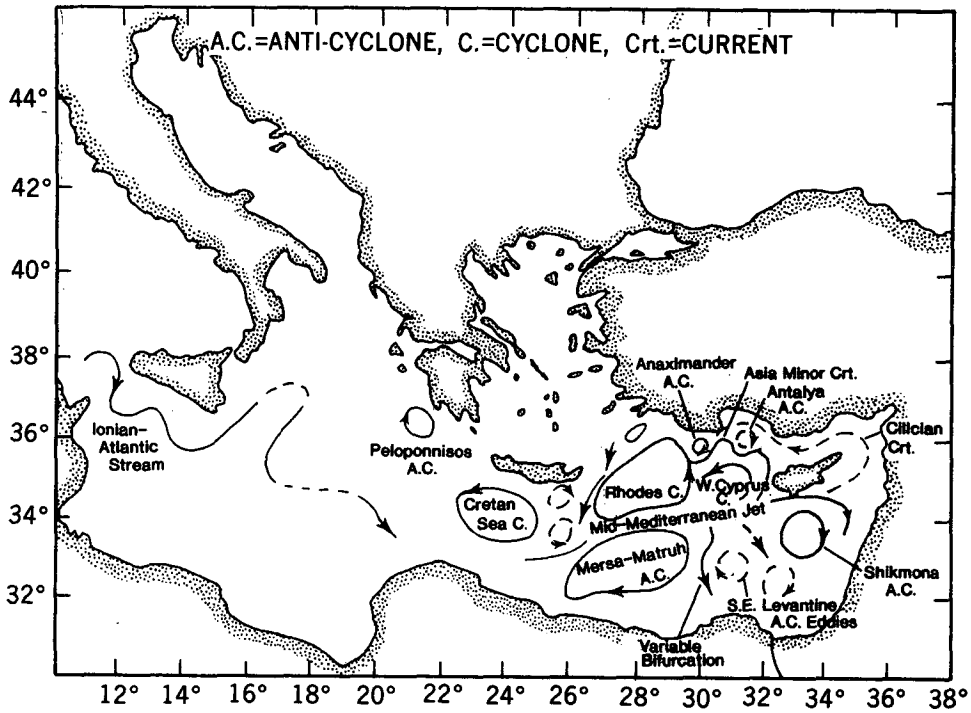

FIG. 13. (*Continued*) (b) Schematic of the EMED circulation (adapted from Robinson et al. 1991).

basin, following a path very similar to that observed by Bignami et al. (1990). The upwelling return flow in Fig. 11 is seen, in Fig. 12, to occur in the eastern portions of the Ionian Sea; the flow then upwells to the surface waters of the Adriatic. Bottom water is obviously created at the surface only in winter, but the general thermohaline circulation is fairly steady throughout the year.

Figure 12 also reveals some formation of bottom water in the Aegean and in portions of the Gulf of Lions and the North Balearic Sea. Upwelling regions are seen along the southern coast of Sicily and in the Levantine Basin.

We could find no evidence of intensive deep mixing of the water column in the northern Balearic Sea. Only a small and limited break in the stratification, extending from the surface to about 250–300-m depth, occurred in winter (not shown) in contrast to the more intense convection structures described by the MEDOC group (1969), Stommel (1972), and Leaman and Schott (1991). The coarse-grid resolution is probably inadequate to capture the dynamics of the MEDOC process, and the use of climatological fluxes to force the model eliminates the strong Mistral bursts that start the deep-water formation (Bunker 1972).

5. The seasonal circulation

a. Background information

The surface and intermediate circulation of the WMED is illustrated in Fig. 13a, according to Millot (1987a,b, 1991). At the surface, the Atlantic water entering the basin forms two anticyclonic gyres in the Alboran Sea (Heburn and La Violette 1990). The eastern side of the eastern Alboran gyre constitutes the Almeria–Oran front (Tintore et al. 1988; Arnone et al. 1990), a strong density contrast between the inflowing Atlantic water and the resident water of the Mediterranean that deflects the MAW flow toward the African coast and originates the Algerian Current flowing along the Algerian coast between 0° and 2°E. The current becomes progressively unstable and generates cyclonic and anticyclonic mesoscale eddies. Observations (Millot 1985) show that only the anticyclonic eddies survive, increase in size, propagate eastward, and can leave the coast and drift into the Balearic Basin. Thus, the MAW not only flows eastward toward the Strait of Sicily but can be advected northward by the eddies, finally coming in contact with more modified MAW at the north Balearic front.

The LIW circulation in the WMED has been the subject of many studies and speculations. It is accepted that, at the exit of the Strait of Sicily, the LIW turns around the western tip of Sicily into the Tyrrhenian Sea where it flows cyclonically along the Italian coast. Before entering the Ligurian Sea, the LIW current originates a branch flowing south and subsequently turning north around Sardinia. According to Wust (1961) and Ovchinnikov (1966), the LIW exiting the Tyrrhenian Sea originates a farther branch proceeding directly westward to the Strait of Gibraltar, explaining

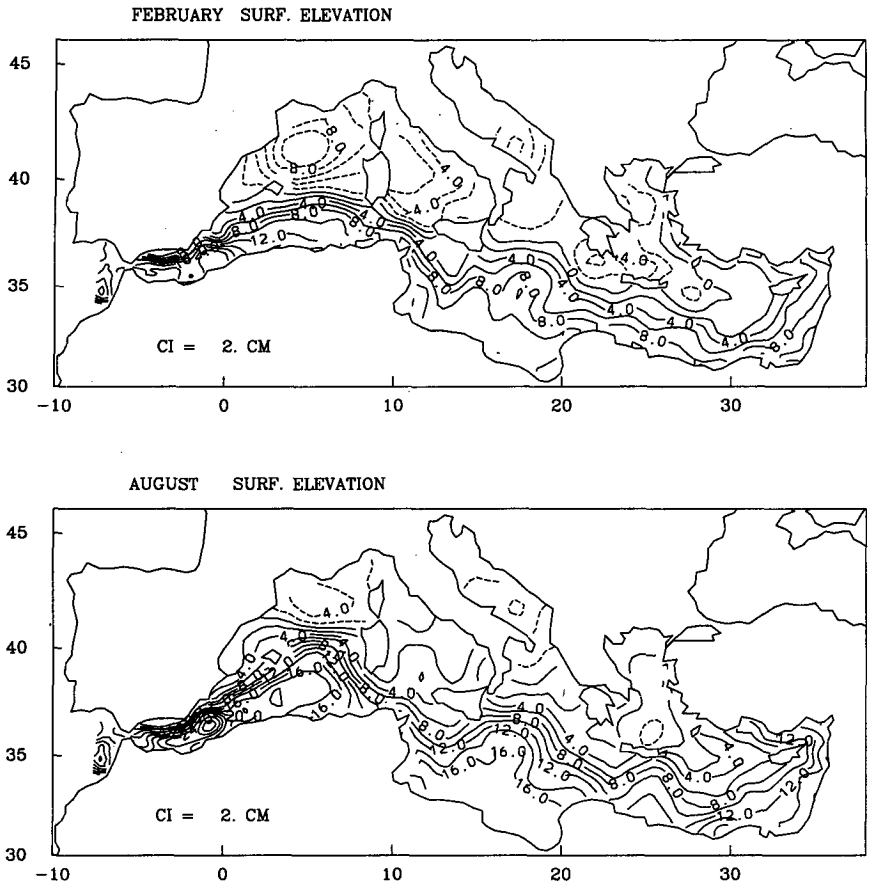

FIG. 14. Surface elevation. (Upper) February; (lower) August. Contour interval is 0.02 m.

the presence of an LIW layer off the North African coast. This view has been questioned by Katz (1972) and Millot (1985) on the basis of field studies and simple theory. The LIW presence in the Algerian Basin is now believed to result from sporadic erosion of the LIW current by mesoscale eddies originating from the Algerian Current.

The circulation of the EMED, relative to the upper thermocline (Robinson et al. 1991), is shown in Fig. 13b. The general circulation appears to be dominated by subbasin gyres interconnected by jets. The MAW enters the EMED and flows through the Ionian Sea (Ionian–Atlantic Stream) into the Levantine Sea (Mid-Mediterranean Jet), where the following gyres are present throughout the year (Özsoy et al. 1989; 1991): a cyclonic gyre between Rhodes and Cyprus (Rhodes gyre) and one south of Crete (Cretan gyre), an anticyclonic gyre off the coast of Egypt (Mersa–Matruh gyre), and a wide anticyclonic area in the northeastern Levantine Basin, the Shikmona eddy. The Mid-Mediterranean Jet flows between the Rhodes and the Mersa–Matruh gyres and then bifurcates twice, east and west of Cyprus. The northward branch originating west of Cyprus feeds the Asia Minor Current, while the southward branch enters the southeastern Levantine anticyclonic region. Although not shown in Fig. 4, another permanent feature in the EMED circulation is the southern Adriatic cyclonic gyre (Malanotte-Rizzoli and Hecht 1988).

b. Model results

The free surface elevation, horizontal streamfunction, and velocity fields for the months of February and August are shown in Figs. 14–17, respectively. The surface circulation in the WMED is dominated by the cyclonic circulation in the Northern Balearic Basin and by the MAW inflow along the north African coast, which feeds the flow into the EMED. In the Alboran Sea two small anticyclonic eddies are formed close to the Moroccan coast, whereas the main flow of the Atlantic water is in the north. Immediately east of the Alboran Sea, the model generates a large and intense anticyclonic eddy, particularly in summer. In the literature there is little evidence of such a feature, an exception being the work of Green and Price (1991), whose results show the occasional formation of an anticyclonic eddy associated with the Almeria–Oran

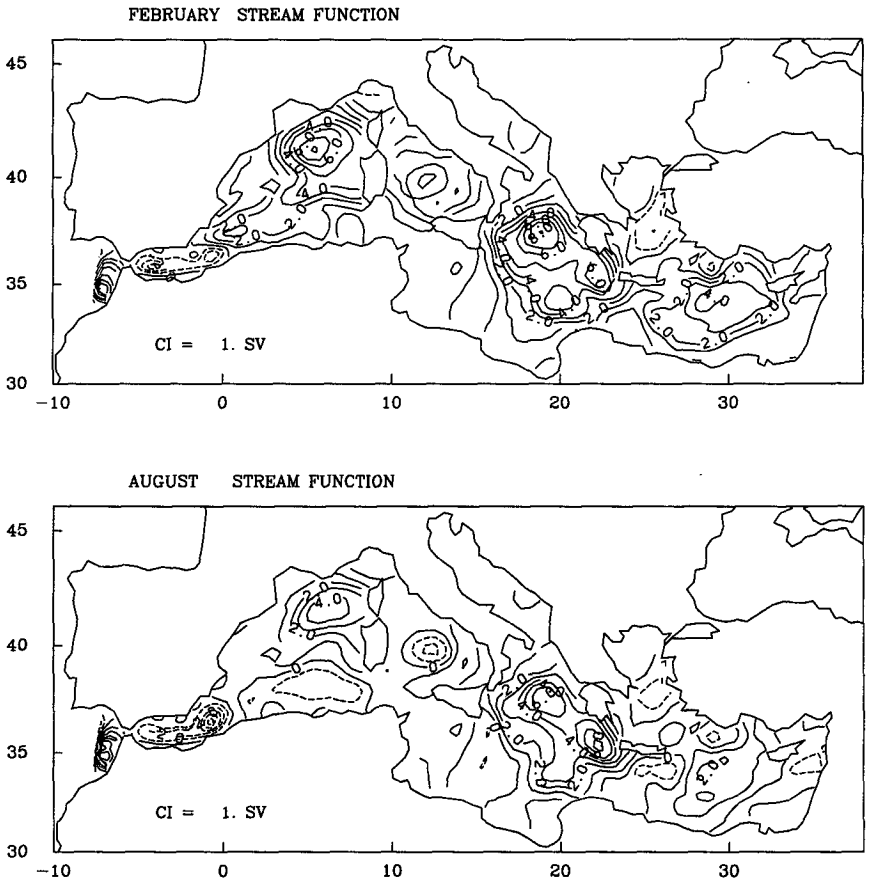

FIG. 15. Horizontal streamfunction. (Upper) February; (lower) August. Contour interval is 1 Sv = 1×10^6 m^3 s^{-1}.

front. It is interesting to note that, in the summer, the surface flow in the Southern Balearic Basin is characterized by the northward shift of the MAW inflow, and it seems that the model attempts to reproduce some features of the Algerian Current behavior leading to the formation of the anticyclonic eddies.

In the Tyrrhenian Sea, the winter circulation is cyclonic, with the MAW feeding a well-developed northward current along the Italian coast. In summer, the interior of the basin shows, in agreement with the observations of Krivosheya and Ovchinnikov (1973) and Tait (1984), a reversal of the circulation from cyclonic to anticyclonic, while weaker flows still persist along Italy and in a smaller cyclonic gyre in the northernmost part of the sea. A consequence of such a reversal is the reduced MAW inflow into the Tyrrhenian Sea.

The MAW stream enters the EMED via the Strait of Sicily and flows into the Ionian Sea forming a wide anticyclonic meander extending from Sicily almost to the entrance of the Cretan Passage. The path of the stream is more complicated in winter than in summer, but there is not a pronounced seasonal variability. The northern portion of the Ionian Sea is occupied by a cyclonic gyre, more intense in winter and weaker in summer, which entrains part of the Ionian–Atlantic stream flow and exchanges water with the permanent cyclonic gyre located in the northern Adriatic Sea. The persistence of the cyclonic gyre in the northern Ionian constitutes one of the major differences between the results of our model and the seasonal maps of the Mediterranean climatological circulation obtained by Tziperman and Malanotte-Rizzoli (1991) using an inverse model. Their results do show a seasonal reversal of the circulation similar to that which we obtained in one of the sensitivity experiments described in the appendix.

In the Levantine Sea a meandering jet comparable to the Mid-Mediterranean Jet exits the Cretan Passage and flows east, bordering a wide cyclonic gyre comparable to the Rhodes gyre. Subsequently, the jet turns north and bifurcates east and west of Cyprus in two branches, both feeding the Asia Minor Current flowing westward along the Turkish coast and merging with the northern side of the Rhodes gyre. In the southern Levantine Basin there is only a hint of a Mersa–Matruh anticyclonic gyre. Another absent feature is the Shik-

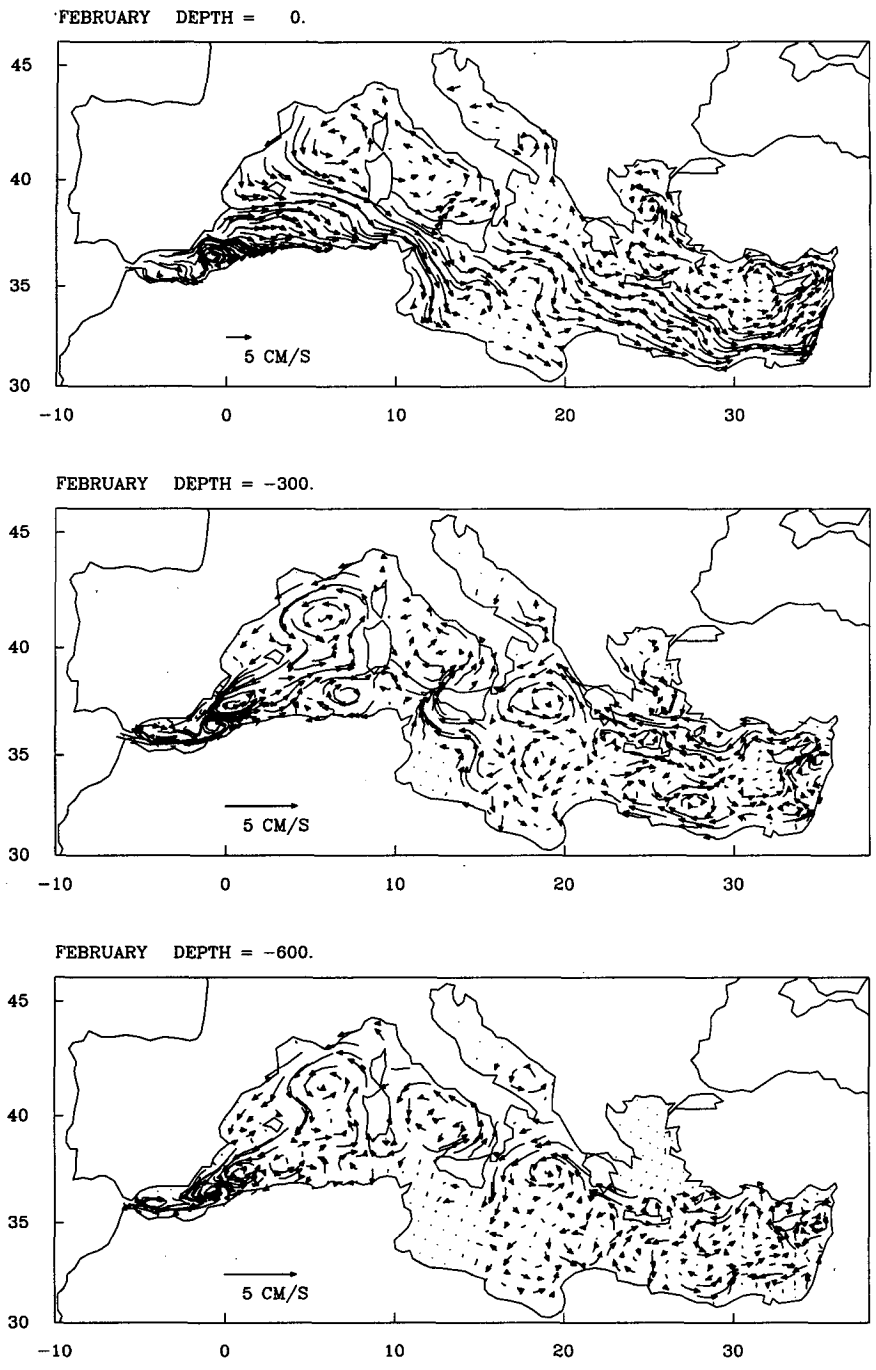

FIG. 16. Velocity trajectories for February: (Upper) 0-m depth with 30-day trajectories; (Middle) 300-m depth with 90 day trajectories; (Lower) 600-m depth with 90-day trajectories.

mona gyre; only a small anticyclonic meander appears seaward of the Israeli coast. The EMED model developed by Malanotte-Rizzoli and Bergamasco (1991) exhibits the same behavior. They attributed this model deficiency to the May (1982) surface heat fluxes, which they thought to be underestimated. This might be the case, but the absence of the Shikmona gyre could be attributed also to the poor resolution of the Eratosthenes Seamount (Brenner et al. 1991) or to interannual variability of the surface forcings as proposed by Hecht (1992).

The intermediate seasonal circulation at depths of 300 and 600 m is shown in Figs. 16, 17. In the EMED there are seasonal differences in the origin of the LIW

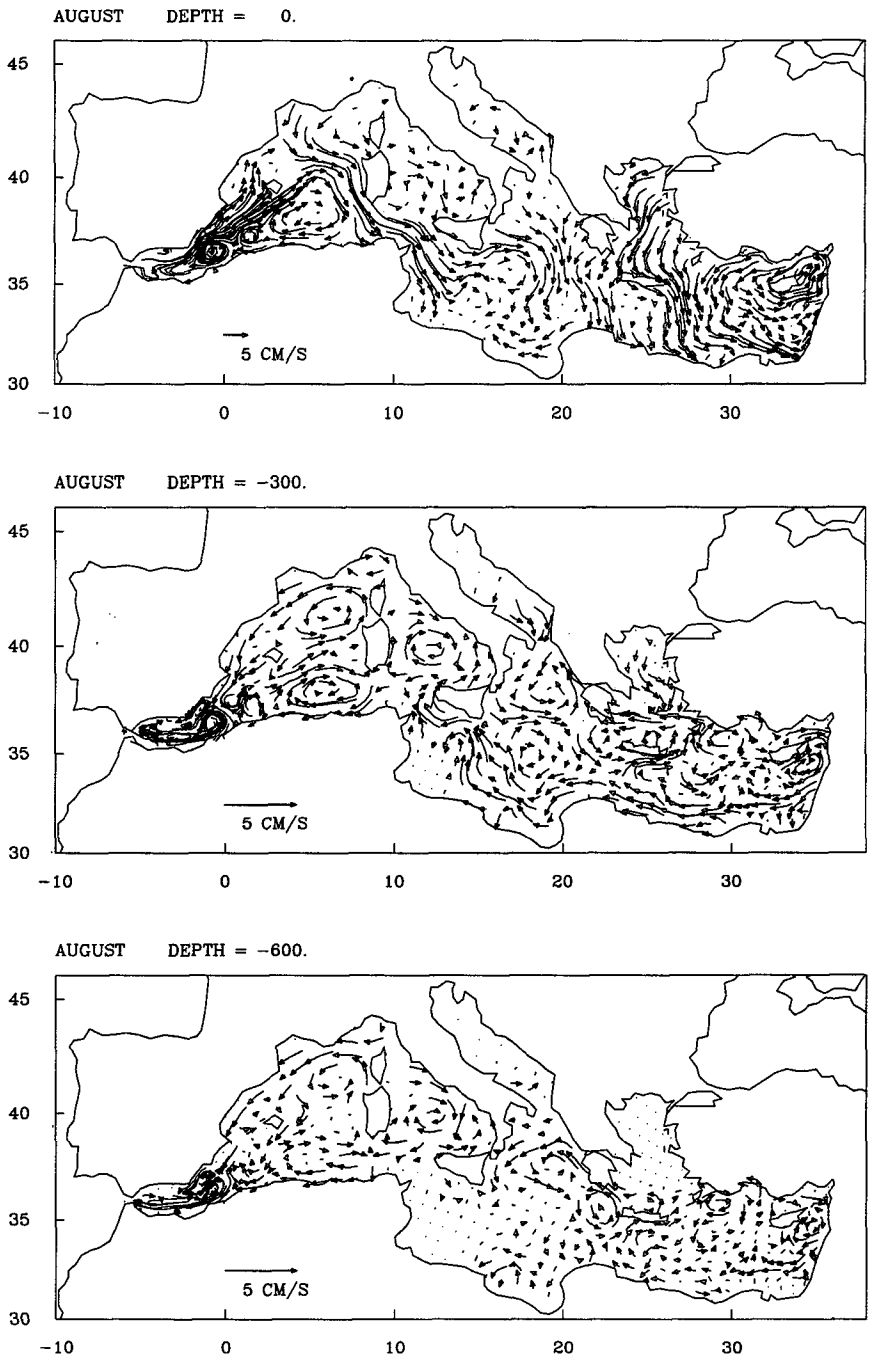

FIG. 17. Velocity trajectories for August. (Upper) 0-m depth with 30-day trajectories. (Middle) 300-m depth with 90-day trajectories. (Lower) 600-m depth with 90-day trajectories.

flow into the WMED. In winter, two currents, coming from the northern and southern Ionian, join south of Sicily to form the outflow, and there is not a direct contribution from the Levantine Sea, as the LIW exiting the basin recirculates in the anticyclonic gyre located in the Cretan Passage. In summer the flow along the eastern coast of Sicily weakens, the anticyclonic gyres in the Cretan Passage and in the Central Ionian become interconnected, and the LIW leaves the Levantine directly flowing from the Cretan Passage to the Strait of Sicily. In the Northern Ionian and in the Southern Adriatic the circulation is cyclonic over the entire year. The center of the Levantine Basin is occupied by a weak cyclonic gyre and east of Rhodes an

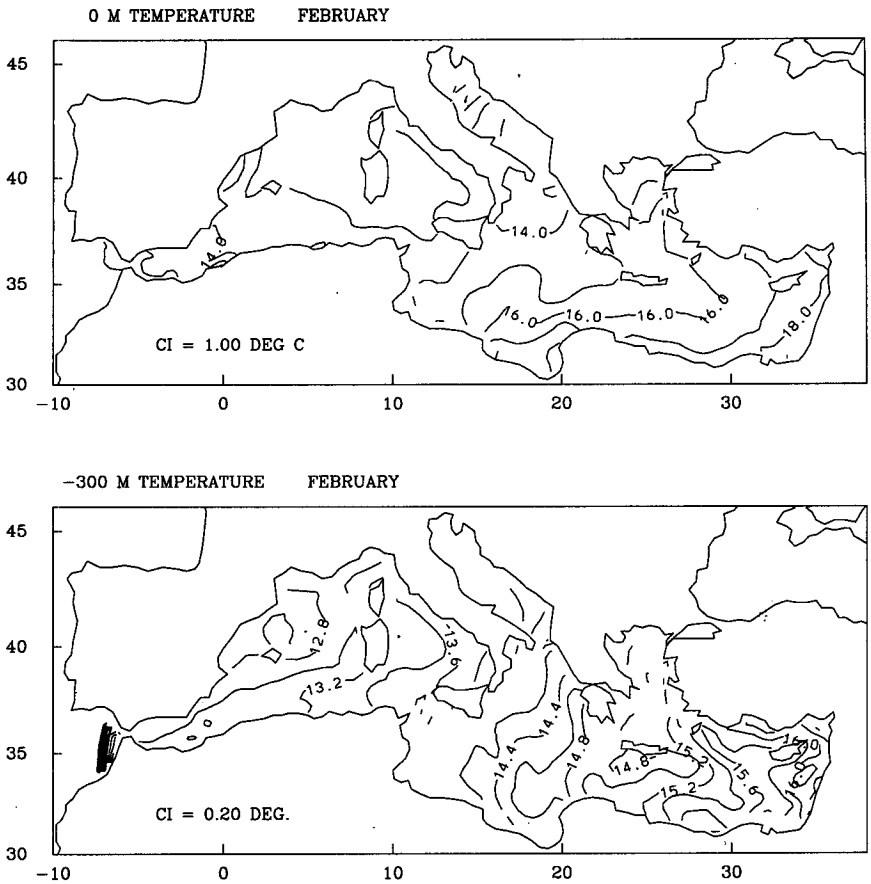

FIG. 18. Temperature distribution for February. (Upper) the surface; the contour interval is 1°C. (Lower) 300 m; the contour interval is 0.2°C.

anticyclone similar to the Anaximander gyre is developed in summer.

In the WMED, the flow patterns look very similar to that proposed by Millot (1985), as described in the background section. The LIW return flow from the EMED crosses the Strait of Sicily and turns around Sicily entering the cyclonic circulation of the Tyrrhenian Sea, from which the LIW exits, then flows around Sardinia, circulates in the northern Balearic Sea cyclonic gyre, and reaches the Alboran Sea moving along the French and Spanish coast. In summer, the Tyrrhenian circulation reverses, and the LIW flow partially bypasses the Tyrrhenian Basin.

The circulation at 1200-m depth is stable throughout the year (not shown) and in the WMED is characterized by a cyclonic pattern in the northern Balearic Basin and by a double gyre in the Tyrrhenian. In the EMED the deep circulation is dominated by the two cyclonic flows in the Ionian Sea and in the Levantine Basin.

Figures 18, 19 show the surface temperature distribution for the months of February and August at the surface and at 300-m depth. The winter surface temperature ranges from about 13°C in the WMED to about 18°C in the EMED. A rough estimate is that model surface temperatures are about 0.5°C too cool in the west with much smaller error in the east. In summer, there is more variability in the surface temperature, ranging from about 20°C to 30°C with warmer temperatures prevailing in the west. The temperatures are in general agreement with the observations (ENEA 1990), but the model appears to be too cool by a degree or more in the northern WMED. In the EMED, the surface temperature values are higher than the observations by about 0.5°C or less (Anati 1977; Ovchinnikov 1984).

The surface salinity fields are shown in Figs. 20, 21. In winter, values range from about 37 psu in the WMED to 39 psu in the EMED. In the summer, there is little change in the west whereas the surface salinities increase by about 0.4 psu in the EMED. All of this seems to be in general accord with observations, an exception being that the model appears to be too fresh by about 0.5 psu in the northern WMED.

In the surface field, the MAW inflow in the southern Balearic Basin is evident throughout the year as a progressive increase of the salinity from west to east. However, in the Balearic Basin, the MAW inflow path moves northward in the summer, as indicated by the

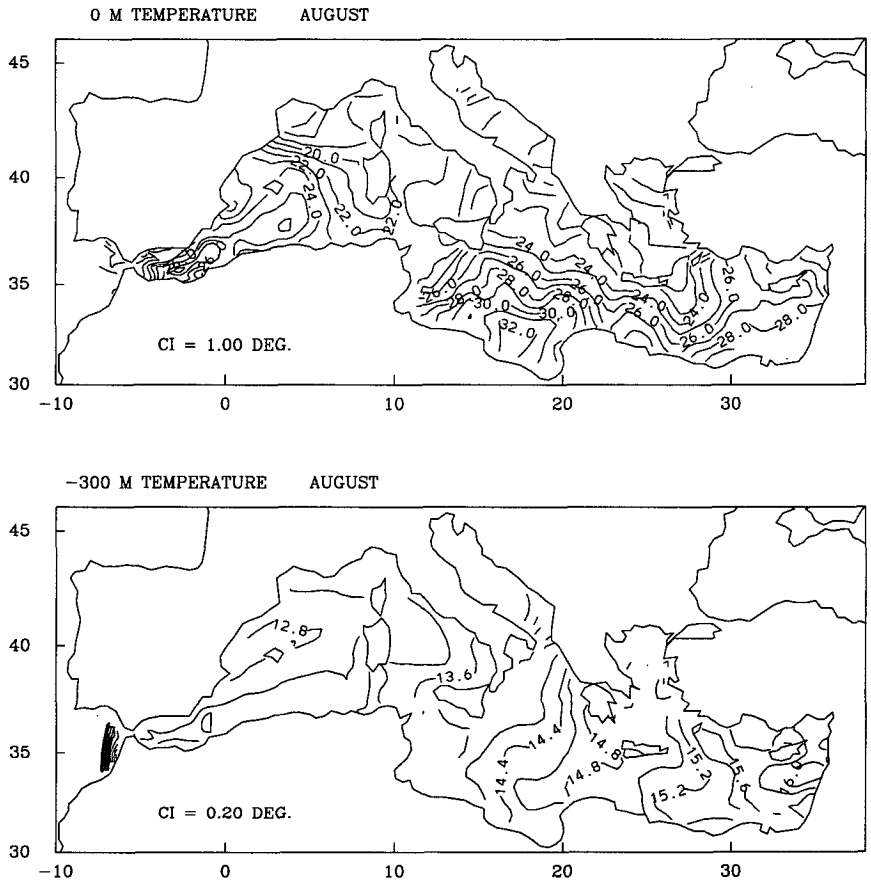

FIG. 19. Temperature distribution for August. (Upper) the surface; the contour interval is 1°C. (Lower) 300 m; the contour interval is 0.2°C.

northward displacement of the isohalines that tend to group in the area between the Balearic Islands and Sardinia, giving hints of the formation of a structure similar to the north Balearic front. To the north, the salinity distribution reflects the cyclonic circulation.

The temperature and salinity horizontal distribution at 300-m depth in February and August reflects the circulation patterns described above; in particular, the temperature field clearly shows the cyclonic circulation in the northern Balearic Sea and the LIW outflow in the Cretan Passage, whereas the salinity fields reflect the anticyclonic circulation in the Ionian Sea.

6. Discussion and conclusions

During the first few years of the model integration, the heat and salinity transport through the Strait of Gibraltar were quite robust as was the entire flow structure. To eliminate the average tendency of temperature and salinities, the surface fluxes analyzed by May (1982) were adjusted by constant values. The model was integrated for 10 years, and the flow and thermodynamic structure were examined in the tenth year.

The general circulation seems to mimic the known structure of the Mediterranean and includes surface inflow and bottom outflow in the Strait of Gibraltar, penetration of MAW through the EMED, across the Strait of Sicily, and into the Levantine Sea. The MAW flow is characterized by the observed summer development of a subsurface salinity minimum. In the Levantine Sea, the MAW is converted into LIW through wintertime mixing created by surface cooling and year long evaporation; it returns along the northern borders of the EMED to the Strait of Sicily. Once through the strait, LIW carves a circuitous route comprised of two major wintertime cyclonic gyres in the Tyrrhenian and Balearic Seas, separated by Sardinia and Corsica. However, in summer, the gyre in the Tyrrhenian Sea reverses and greatly reduces the LIW flow into that basin. Thus, it seems that the LIW circulation oscillates between a winter configuration similar to the hypothesis put forward by Millot (1987b), involving circulation in the Tyrrhenian Sea and a summer configuration more in agreement with Katz (1972), who posits a direct flow of the LIW into the Balearic Basin along the western coast of Sardinia.

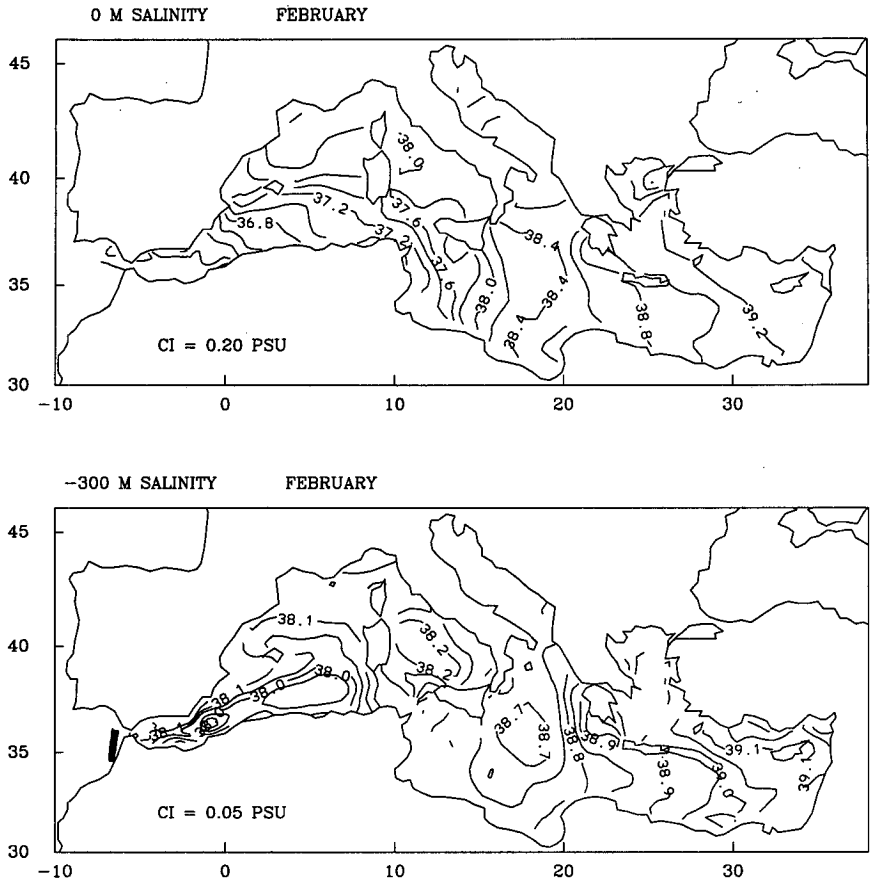

FIG. 20. Salinity distribution for February. (Upper) the surface; the contour interval is 0.20 psu. (Lower) 300 m; the contour interval is 0.50 psu.

Winter surface fluxes and subsequent mixing in the Adriatic Sea provide a source of deep water to the EMED, advecting to the abyss in intense, bottom-trapped currents. Similar bottom water sources appear in the Aegean. The presence of the deep-water formation in the Adriatic Sea creates a realistic simulation of the EMED thermohaline circulation, which, in agreement with the findings of the POEM Group (1992), is formed by an open cell of circulation consisting of the MAW/LIW system and by a deeper closed cell fed by the dense water outflow from the Adriatic and closed by ascending branches in the Ionian Sea and the Levantine Basin.

In the WMED, bottom water is formed in the northern shallow region of the Balearic Sea. The model did not produce localized "chimney" structures in the northern Balearic Sea, possibly due to insufficient horizontal resolution and the use of climatological surface forcing fields.

In the Levantine Sea, the surface circulation consists of subregional gyres of both sign interconnected by the Mid-Mediterranean Jet and the Asia Minor Current. All the experiments performed reproduced the Rhodes gyre, the bifurcation of the Mid-Mediterranean Jet east and west of Cyprus and the Asia Minor Current. However, the Mersa–Matruh and Shikmona anticyclonic gyres were absent or not correctly reproduced. Such features appear in the geostrophic computations based on the quasi-synoptical data of the POEM project (Özsoy et al. 1989; 1991). This discrepancy between model and observations indicates a possible underestimation of the surface heat and salinity fluxes in the Levantine Sea area.

At intermediate depths the LIW outflow through the Strait of Sicily is reproduced well by the model. The LIW path across the EMED undergoes seasonal changes, particularly in the connecting flow between the Levantine and the Ionian Seas, across the Cretan Passage, which appears reduced in winter. The LIW Current in the Ionian is entrained in the anticyclonic cell located in the center of the Basin and before entering the Strait of Sicily mixes further with water coming from the northern Ionian Sea.

In the WMED, the surface circulation in the Balearic Basin is characterized by a cyclonic circulation in the north, by the MAW inflow in the south, and by a seasonal reversal of the circulation in the Tyrranean Sea.

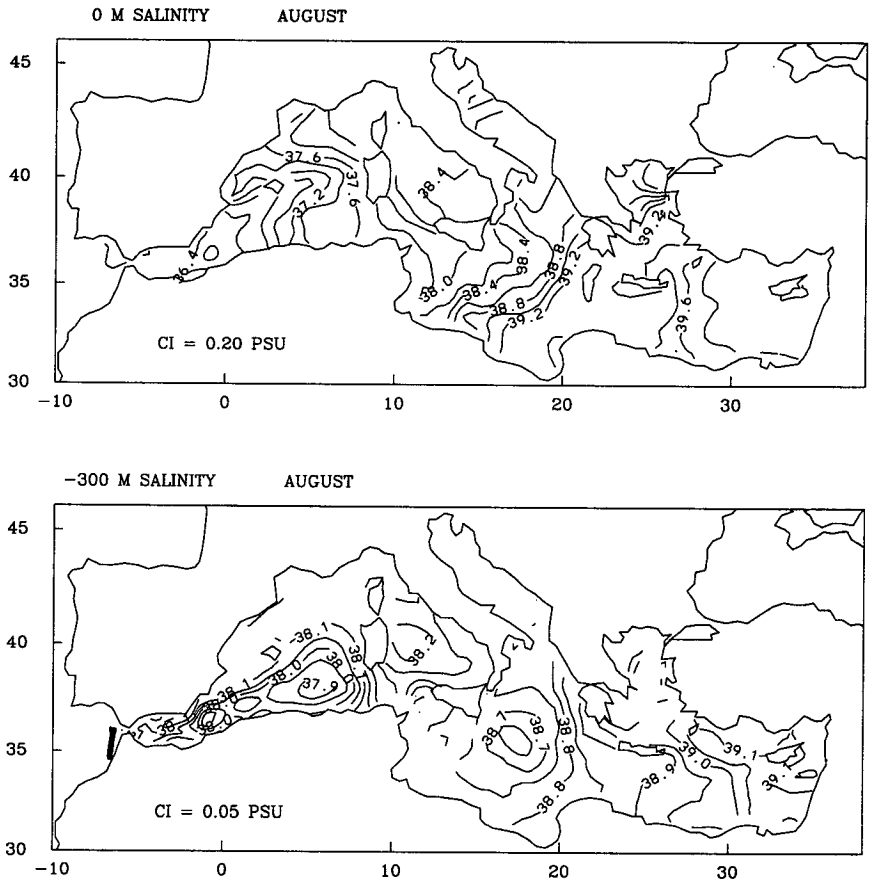

FIG. 21. Salinity distribution for August. (Upper) the surface; the contour interval is 0.20 psu. (Lower) 300 m; the contour interval is 0.50 psu.

The results of the central experiment and additional experiments described in the appendix as well as the results of other modeling efforts (Heburn 1987; Pinardi and Navarra 1993) indicate that, in general, the wind stress seasonality is a very important forcing factor. However, the temporal and spatial variability in the surface salinity flux and the effect of fresh water runoff are necessary for the maintenance of a realistic horizontal density gradient that drives the cyclonic circulation in the northern Balearic Basin. Moreover, the seasonal surface buoyancy flux seems to have an enhancing effect on the summer generation of the anticyclonic mesoscale eddies in the south and strengthens the seasonal reversal of the circulation in the Tyrrhenian Sea that extends from the surface to the intermediate layers.

A general conclusion is that the model seems to do a fairly good job of simulating the dynamics and thermodynamics of the Mediterranean. Undoubtedly, future calculations will profit from higher resolution and longer run times. Current structures would probably be narrower. Since bottom flows seem to be important in the Mediterranean, one should add more vertical grid points near the bottom and actually resolve the boundary layer. And, it would be useful to evaluate the relative importance of the bottom boundary layers with more extensive diagnostics and software. We have used the model to infer information on the overall heat and salinity budget. Possibly, this approach might be extended to supply more detailed information on surface forcing. In fact, the Mediterranean Sea would seem to be a very nice vehicle on which to test climate modeling ideas.

Acknowledgments. The support of the New Jersey Marine Science Consortium and the Agency for International Development under Contract NEB-0158-G-SS-5192-00 "A study of the circulation of the Levantine Basin" and the support of NOAA's Geophysical Fluid Dynamics Laboratory are gratefully acknowledged. G. W. Heburn, S. Brenner, and R. Slater kindly provided us with wind stress, surface heat fluxes, and precipitation data and I. A. Maiyza provided the annually averaged hydrological climatologies with which we initialized the model. Help and advice during the initial phase of this study were obtained from S. Levitus and

TABLE A.1. Characteristics of the numerical experiments.

Experiment	Wind stress	Thermal surface condition	Salinity surface condition	River runoff
I	Monthly	Surface temperature equal to initial conditions	Surface salinity equal to initial conditions	No
II	Monthly	Monthly heat flux	Constant salinity flux	No
III	Monthly	Monthly heat flux	Surface salinity equal to initial conditions	No
IV	Monthly	Monthly heat flux	Monthly salinity flux	Annual

M. Jackson. During a substantial revision process, support was provided by the Office of Naval Research under Grant N00014-93-1-0037.

APPENDIX

Surface-Forcing Sensitivity

We give here a brief description of the numerical experiments performed using different kinds of surface forcings. Their characteristics are summarized in Table A.1. Experiment IV is the central experiment described above.

The integration time was 5 years for experiments I, II, and III, and 10 years for experiment IV.

a. Experiment I

In this experiment the model was forced with the monthly wind stress climatologies, while the surface temperature and salinity were prescribed to be equal to the annual average (initial conditions) to simulate perpetual annual average conditions in the surface fluxes. Thus, we examine the effects of the seasonal wind forcing by eliminating any seasonality in the surface heat and salinity fluxes. The circulation pattern developed in the whole Balearic Sea was similar to the pattern produced in the central experiment. On the other hand, the Tyrrhenian Sea circulation did not show the summer reversal but only a weakening of the cyclonic flow.

In the EMED the major differences with respect to the central experiment concerned the Ionian–Atlantic Stream, which showed a strong seasonal variability. In winter, at the exit of the Strait of Sicily, the stream bifurcates into two branches: one closely following the African coast and directly entering the Levantine Basin, the other meandering in the central Ionian Sea. In summer the coastal branch reverses and the second branch is shifted north. In the northern Ionian the winter cyclonic circulation reverses to anticyclonic in summer. Other differences arose in the Levantine Sea, particularly in summer; the model developed two very weak anticyclonic gyres, approximately at the same location of the Mersa–Matruh and Shikmona gyres.

b. Experiment II

The model was forced by monthly averaged wind stress and heat flux. The surface salinity flux was constant in time and space and was obtained by prescribing a surface freshwater flux of 1 m yr^{-1}, corresponding to the estimated W_S average for the whole Mediterranean Sea (Bethoux 1979).

Despite the use of a more realistic surface forcing, the results of experiment II were not entirely satisfactorily. The major problem was that, after five years of integration, the cyclonic circulation in the northern Balearic Basin almost disappeared. Furthermore, the anticyclonic area developed in summer by the central experiment (as well as by experiment I) was ill defined.

The circulation features in the EMED were more satisfactory and comparable with the results of experiment I.

c. Experiment III

To understand if the problem in the Northern Balearic Basin was caused by the surface heat or salinity flux, experiment III was carried out whereby the model was driven with monthly wind stress and surface heat flux, but the surface salinity was maintained equal to the initial conditions. The use of such forcing maintained the cyclonic circulation in the northern Balearic Sea and confirmed that the choice of a constant salinity flux was overly simplistic and that the salinity flux is a very important factor in determining Mediterranean circulation features.

REFERENCES

Anati, D. A., 1977: Topics in the physics of the Mediterranean Seas. Ph. D. thesis, Weizmann Institute of Science, 43 pp.

——, 1984: A dome of cold water in the Levantine Basin. *Deep-Sea Res.*, **31**, 1251–1257.

Arnone, R. A., D. A. Wiesenburg, and K. D. Saunders, 1990: The origin and characteristics of the Algerian Current. *J. Geophys. Res.*, **95**, 1587–1598.

Artegiani, A., and E. Salusti, 1987: Field observation of the flow of dense water on the bottom of the Adriatic Sea during the winter 1981. *Oceanol. Acta.*, **10**, 387–391.

Beckers, J. M., 1991: Application of the GHER 3D general circulation model to the western Mediterranean. *J. Mar. Sys.*, **1**, 315–322.

Bergamasco, A., P. Malanotte-Rizzoli, W. C. Thacker, and R. B. Long, 1993: The seasonal steady circulation of the Eastern Mediterranean determined with the adjoint method. *Deep-Sea Res.*, **40**(6), 1269–1298.

Bethoux, J. P., 1979: Budgets of the Mediterranean Sea. Their dependence on the local climate and on the characteristics of the Atlantic waters. *Oceanol. Acta*, **2**, 157–163.

Bignami, F., E. Salusti, and S. Schiarini, 1990: Observations of a vein of dense water in the Southern Adriatic and Ionian Sea. *J. Geophys. Res.*, **95**, 7249–7259.

Blumberg, A. F., and G. L. Mellor, 1983: Diagnostic and prognostic numerical circulation studies of the South Atlantic Bight. *J. Geophys. Res.*, **88,** 4579–4592.

——, and ——, 1987: A description of a three-dimensional coastal ocean circulation model. *Three-Dimensional Coastal Ocean Models, Coastal Estuarine Science,* N. S. Heaps, Ed., Amer. Geophys. Union, 1–16.

Brenner, S., Z. Rozentraub, J. Bishop, and M. Krom, 1991: The mixed-layer/thermocline cycle of a persistent warm core eddy in the eastern Mediterranean. *Dyn. Atmos. Oceans,* **15,** 457–476.

Bunker, A., 1972: Wintertime interactions of the atmosphere with the Mediterranean Sea. *J. Phys. Oceanogr.*, **2,** 225–238.

ENEA, 1990: *Climatological Atlas of the Western Mediterranean.* Santa Teresa Center for Energy and Environmental Research, 224 pp.

Galperin, B., and G. L. Mellor, 1990a: A time-dependent, three-dimensional model of the Delaware Bay and River. Part 1: Description of the model and tidal analysis. *Estuarine Coastal Shelf Sci.*, **31,** 231–253.

——, and ——, 1990b: A time-dependent three-dimensional model of the Delaware Bay and River. Part 2: Three dimensional flow fields and residual circulation. *Estuarine Coastal Shelf Sci.*, **31,** 255–281.

Garrett, C., R. Outerbridge, and K. Thompson, 1993: Interannual variability in Mediterranean heat and buoyancy fluxes. *J. Climate,* **6,** 900–910.

Gilman, C., and C. Garrett, 1994: Heatflux parameterization for the Mediterranean Sea: The role of atmospheric aerosols and constraints in the water budget. *J. Geophys. Res.*, **99,** 5119–5134.

Green, D. W., III, and J. A. Price, 1991: Buoy tracks and circulation in the western Mediterranean. *Proc. Conf. MTS '91,* New Orleans, LA. Mar. Technol. Soc. 876–882.

Harzallah, A., D. L. Cadet, and M. Crepon, 1993: Possible forcing effects of net evaporation, atmospheric pressure and transients on water transport in the Mediterranean Sea. *J. Geophys. Res.*, **98,** 12 341–12 350.

Heburn, G. W., 1987: The dynamics of the western Mediterranean Sea: A wind forced case study. *Ann. Geophys.*, **5B,** 61–74.

——, and P. E. La Violette, 1990: Variations in the structure of the anticyclonic gyres found in the Alboran Sea. *J. Geophys. Res.*, **95,** 1599–1613.

Hecht, A., 1992: Abrupt changes in the characteristics of Atlantic and Levantine intermediate waters in the Southeastern Levantine Basin. *Oceanol. Acta,* **15,** 25–42.

Hopkins, T. S., 1978: Physical processes in the Mediterranean Basins. *Estuarine Transport Processes,* B. Kjerfve, Ed., University of South Carolina Press, 269–310.

——, 1985: Physics of the Sea. *Western Mediterranean,* R. Margalef, Ed., Pergamon Press, 100–125.

Jaeger, L., 1976: Monatskarte des niederschlags fur die ganze Erde. Ber. Dtsch. Wetterdienstes, Band 18, No. 18, 39 pp.

Jerlov, N. G., 1976: *Marine Optics.* Elsevier Science, 231 pp.

Katz, E. J., 1972: The Levantine Intermediate water between the Strait of Sicily and the Strait of Gibraltar. *Deep-Sea Res.*, **19,** 507–520.

Kinder, T. H., and G. Parrilla, 1987: Yes, some of the Mediterranean outflow does come from great depth. *J. Geophys. Res.*, **92,** 2901–2906.

Krivosheya, V. G., and I. M. Ovchinnikov, 1973: Peculiarities in the geostrophic circulation of the waters of the Tyrrhenian Sea. *Oceanol.*, **12,** 822–827.

Lacombe, H., and P. Tchernia, 1960: Quelques trait generaux de l'hydrologie Méditerranéenne. *Cah. Oceanogr.*, **12,** 525–547.

Lascaratos, A., R. G. Williams, and E. Tragou, 1993: A mixed-layer study of the formation of Levantine Intermediate Water. *J. Geophys. Res.*, **98,** 14 739–14 749.

Leaman, K. D., and A. Hecht, 1988: Large-scale properties of the eastern Mediterranean: A review. *Oceanol. Acta,* **11,** 323–335.

——, and F. A. Schott, 1991: Hydrographic structure of the convection regime in the Gulf of Lions: Winter 1987. *J. Phys. Oceanogr.*, **21,** 575–598.

Malanotte-Rizzoli, P., and A. Bergamasco, 1989: The general circulation of the eastern Mediterranean. Part I: The barotropic wind-driven circulation. *Oceanol. Acta,* **12,** 335–351.

——, and ——, 1991: The wind and thermally driven circulation of the eastern Mediterranean Sea. Part II: The baroclinic case. *Dyn. Atmos. Oceans,* **15,** 355–419.

May, P. W., 1982: Climatological flux estimates in the Mediterranean Sea: Part I. Winds and wind stresses. NORDA Tech. Rep., Vol. 54, 58 pp.

MEDOC Group, 1969: Observation of formation of deep water in the Mediterranean Sea. *Nature,* **227,** 1037–1040.

Mellor, G. L., 1991a: User's guide for a three dimensional, primitive equation, numerical ocean model. AOS Program Rep., Princeton University, Princeton, NJ, 34 pp.

——, 1991b: An equation of state for numerical models of oceans and estuaries. *J. Atmos. Oceanic Technol.*, **8,** 609–611.

——, and T. Yamada, 1982: Development of a turbulent closure model for geophysical fluid problems. *Rev. Geophys.*, **20,** 851–875.

——, and A. F. Blumberg, 1985: Modeling vertical and horizontal diffusivities with the sigma coordinate system. *Mon. Weather Rev.*, **113,** 1279–1383.

——, and T. Ezer, 1991: A Gulf Stream model and an altimetry assimilation scheme. *J. Geophys. Res.*, **96,** 8779–8795.

Menzin, A. B., and L. V. Moskalenko, 1982: Calculation of wind-driven currents in the Mediterranea Sea by the electrical simulation method (homogeneous model). *Oceanol.*, **22,** 537–540.

Millot, C., 1985: Some features of the Algerian current. *J. Geophys. Res.*, **90,** 7169–7176.

——, 1987a: The circulation of the Levantine Intermediate Water in the Algerian Basin. *J. Geophys. Res.*, **92,** 8265–8276.

——, 1987b: Circulation in the western Mediterranean Sea. *Oceanol. Acta,* **10,** 143–149.

——, 1991: Mesoscale and seasonal variability of the circulation in the western Mediterranean. *Dyn. Atmos. Oceans,* **15,** 179–214.

Morcos, S. A., 1972: Sources of Mediterranean intermediate water in the Levantine Sea. *Studies in Physical Oceanography, A Tribute to Georg Wust on His 80th birthday,* A. L. Gordon, Ed. Gordon and Breach, 185–206.

Oey, L.-Y., G. L. Mellor, and R. I. Hires, 1985a: A three-dimensional simulation of the Hudson Raritan estuary. Part I: Description of the model and model simulations. *J. Phys. Oceanogr.*, **15,** 1676–1692.

——, ——, and ——, 1985b: A three-dimensional simulation of the Hudson Raritan estuary. Part II: Comparison with observations. *J. Phys. Oceanogr.*, **15,** 1693–1709.

——, ——, and ——, 1985c: A three-dimensional simulation of the Hudson Raritan estuary. Part III, Salt flux analysis. *J. Phys. Oceanogr.*, **15,** 1711–1720.

Ovchinnikov, I. M., 1966: Circulation in the surface and intermediate layers of the Mediterranean Sea. *Oceanology,* **6,** 48–59.

——, 1984: The formation of intermediate water in the Mediterranean. *Oceanology,* **24,** 168–173.

——, V. I. Zats, V. G. Krivosheya, M. S. Nemirosky, and A. I. Udodov, 1987: Winter convection in the Adriatic and formation of deep eastern Mediterranean waters. *Ann. Geophys.*, **5B,** 89–92.

Özsoy, E., A. Hecht, and U. Unluata, 1989: Circulation and hydrography of the Levantine Basin. Results of the POEM coordinated experiments 1985–86. *Progress in Oceanography,* Vol. 22, Pergamon, 125–170.

——, ——, ——, S. Brenner, T. Oguz, J. Bishop, M. A. Latif, and Z. Rozentraub, 1991: A review of the Levantine Basin circulation and its variability during 1985–1988. *Dyn. Atmos. Oceans,* **15,** 421–456.

Pinardi, N., and A. Navarra, 1993: Baroclinic wind adjustment processes in the Mediterranean Sea, *Deep-Sea Res. II,* **40**(6), 1299–1326.

POEM Group, 1992: General circulation of the Eastern Mediterranean. *Earth Sci. Rev.*, **32,** 285–309.

Robinson, A. R., M. Golnaraghi, W. G. Leslie, A. Artegiani, A. Hecht, E. Lazzoni, A. Michelato, E. Sansone, A. Theocaris, and U. Unluata, 1991: The eastern Mediterranean general circulation: Features, structure and variability. *Dyn. Atmos. Oceans,* **15,** 215–240.

Roussenov, V., E. Stanev, V. Artale, and N. Pinardi, 1994: A seasonal model of the Mediterranean Sea general circulation. *J. Geophys. Res.*, in press.

Sankey, T., 1973: The formation of deep water in the northwestern Mediterranean. *Progress in Oceanography,* Vol. 6, Pergamon, 159–179.

Stanev, E. V., H. J. Friedrich, and S. Botev, 1989: On the seasonal response of intermediate and deep water to surface forcing in the Mediterranean Sea. *Oceanol. Acta,* **12,** 141–149.

Stommel, H., 1972: Deep winter convection in the western Mediterranean Sea. *Studies in Physical Oceanography, A Tribute to Georg Wust on His 80th Birthday,* A. L. Gordon Ed. Gordon and Breach, 207–218.

Tait, R. I., 1984: The physical oceanography of the Tyrrhenian and Ligurian Seas. *Proc. Sixth Congresso dell'Associazione Italiano di Oceanologia e Limnologia,* 48–84.

Tintore, J. D., P. E. La Violette, I. Blade, and A. Cruzado, 1988: A study of an intense density front in the eastern Alboran Sea: The Almeria Oran front. *J. Phys. Oceanogr.*, **18,** 1384–1397.

Tziperman, E., and P. Malanotte-Rizzoli, 1991: The climatological seasonal circulation of the Mediterranean Sea. *J. Mar. Res.*, **49,** 411–434.

UNEP, 1984: Pollutants from land-based sources in the Mediterranean. UNEP Regional Seas Reps., Vol. 32, 97 pp.

Wust, G., 1961: On the vertical circulation of the Mediterranean Sea. *J. Geophys. Res.*, **66,** 3261–3271.